Assessment of variability of the thermohaline structure and transport of Atlantic water in the Arctic Ocean based on NABOS CTD data

Nataliya Zhurbas[1] and Natalia Kuzmina[1]

[1]Shirshov Institute of Oceanology, Russian Academy of Sciences, 36 Nakhimovsky Prospekt , 117997 Moscow, Russia

Correspondence to: Nataliya Zhurbas (nvzhurbas@gmail.com)

Abstract. Data of CTD transects across continental slope of the Eurasian Basin and the St. Anna Trough performed during NABOS (Nansen and Amundsen Basins Observing System) project in 2003–2015 were used to assess θ-S characteristics and volume flow rates of the current carrying the Atlantic Water (AW) in the Arctic Ocean. The assessments were based on the analysis of CTD data including 33 sections in the Eurasian Basin, 4 transects in the St. Anna Trough and 2 transects in the Makarov Basin; additionally a CTD transect of the Polarstern-1996 expedition (PS-96) was considered. Using spatial distributions of temperature, salinity, and density along the transects and applying θ-S analysis, the variability of thermohaline pattern on the AW pathway along the slope of Eurasian Basin was investigated. The Fram Strait branch of the Atlantic Water (FSBW) was identified on all transects, including two transects in the Makarov Basin (along 159°E), while the cold waters, which can be associated with the influence of the Barents Sea branch of the Atlantic water (BSBW), on the transects along 126°E, 142°E and 159°E, were observed in the depth range below 800 m and had a negligible effect on the spatial structure of isopycnic surfaces. Special attention was paid to the variability of the geostrophic volume flow rate of the AW propagating along the continental slope of the Eurasian Basin. An interpretation of the spatial and temporal variability of hydrological parameters characterizing the flow of the AW in the Eurasian Basin is presented. The geostrophic volume flow rate decreases significantly farther away from the areas of the AW inflow to the Eurasian Basin. Thus, the geostrophic estimate of the volume rate for the AW flow in the Makarov Basin at 159°E was found to be more than an order of magnitude smaller than the estimates of the volume flow rate in the Eurasian Basin, implying that the major part of the AW entering the Arctic Ocean circulates cyclonically within the Nansen and Amundsen Basins. There is an absolute maximum of θ_{max} (AW core temperature) in 2006–2008 time series and a maximum in 2013, but only at 103°E. Salinity $S(\theta_{max})$ (AW core salinity) time series display an increase of the AW salinity in 2006–2008 and 2013 (at 103°E) that can be referred to as a AW salinization in the early 2000s. The maxima of θ_{max} and $S(\theta_{max})$ in 2006-2008 and 2013 were accompanied by the volume flow rate highs. Additionally the time average volume rates, V_{mean}, were calculated for

the FSBW flow ($V_{mean} = 0.5$Sv in the longitude range 31–92°E), for the BSBW flow in the St. Anna Trough ($V_{mean} = 0.79$ Sv) and for a combined FSBW and BSBW flow in longitude range 94–107°E ($V_{mean} = 1.09$ Sv).

1 Introduction

It is well known (see, e.g., Aagaard, 1981; Rudels et al.,1994; Schauer et al., 1997; Rudels et al., 1999; Schauer et al., 2002a, b; Rudels et al., 2006; Berzczynska-Möller et al., 2012; Rudels et al., 2015; Rudels, 2015; Dmitrenko et al., 2015; Pnyushkov et al., 2015, 2018b) that Atlantic water (AW) enters the Eurasian Basin in two ways: one part originates from the Greenland and Norwegian seas and flows to the Basin through the Fram Strait (Fram Strait branch of the Atlantic Water, hereinafter the FSBW, and the other reaches the deep part of the Arctic Ocean near St. Anna Through after passing through the Barents Sea (Barents Sea branch of the Atlantic water, hereinafter the BSBW. After entering the Eurasian Basin the FSBW forms an eastward subsurface baroclinic boundary current with a core of higher temperature and salinity adjacent to the continental slope. In the longitude range of 80–90°E it encounters and partially mixes with the BSBW, which is strongly cooled due to mixing with shallow waters of the Arctic shelf seas and atmospheric impact (Schauer et al., 1997; 2002a, b). Further, the water masses resulting from the interaction of two branches which transport the AW continue spreading cyclonically in the Eurasian Basin, following the sea bed topography.

To study the characteristics of the FSBW and BSBW flow in the Eurasian Basin, it is useful to estimate, first of all, its volume flow rate in different parts of the Basin. Generally the estimates of the AW volume flow rate have been based on direct current observations (Fahrbach et al., 2001; Berzczynska-Möller et al., 2012; Rudels et al., 2014; Pnyushkov et al., 2015). However, to solve a number of fundamental and climatic problems it is worth considering the AW volume flow rate calculated on the basis of geostrophic velocity estimates. Such estimates, obtained for different regions of the Arctic Basin, were given in a number of papers (e.g. Marnela et al., 2013; Våge et al., 2016; Pérez-Hernández et al., 2017; Kolås and Fer, 2018). Nevertheless, it is of interest to carry out estimates of the AW geostrophic volume flow rate along continental slope of the Eurasion Basin based on a large volume of empirical data.

Within the NABOS (Nansen and Amundsen Basins Observing System) project (Polyakov et al., 2007) a unique volume of CTD data was collected: more than 30 sections were made in various regions of the Arctic Basin in the summer/fall 2002-2015. A number of sections in different years were made in the same regions of the Basin, which allows studying the interannual variability of the water masses thermohaline structure and the geostrophic volume flow rate in these areas.

The main goal of this work is to investigate the spatial and temporal variability of the AW geostrophic volume flow rate during its propagation along the continental slope of the Eurasian Basin. Another important aspect of our analysis is the investigation of the thermohaline structure and transformation of the FSBW and BSBW. Such analysis is essential for two reasons: a) the estimates of the AW transport are sensitive to the temperature and salinity ranges used for the identification of this water (Pnyushkov et al., 2018b); b) it is reasonable to assume that mixing of FSBW, BSBW and surrounding waters may reduce the AW geostrophic volume flow rate. Usually there is no probem in the identification of the FSBW (for details, see (Pnyushkov et al., 2018b)). But this is not the case with the identification of the BSBW: it is difficult to determine which waters flowing out of the St. Anna Trough and the Voronin Trough should be attributed to the BSBW. There are differences in the definition of the BSBW in (Schauer et al., 1997; Schauer et al., 2002a, b) and (Dmitrenko et al., 2015). In section 3.1.1 we will briefly describe the essence of these differences.

2 Material and Methods

We used data of CTD profiling on transects across the slope of the Eurasian Basin in the longitude range of 31–159°E measured in the years 2002–2015 within the framework of NABOS project (in total 39 transects). The data are freely available at the site http://nabos.iarc.uaf.edu. Apart from the NABOS data, a CTD transect across the whole Eurasian Basin and over the Lomonosov Ridge starting at 92°E at the slope from R/V *Polarstern* in 1996 (hereafter PS96) was also included. The locations of the CTD transects are shown in Fig. 1. It can be seen from the map in Fig. 1 that most of the CTD transects are aligned cross-slope and grouped at longitudes of 31, 60, 90, 92, 94, 96, 98, 103, 126, 142, and 159°E. Four of the 40 transects crossed zonally the St. Anna Trough (at the latitude of 81, 81.33, 81.42, and 82°N) through which the BSBW enters the Eurasian Basin. Most of the CTD casts covered the upper layer from the sea surface to either 1000 m depth or to the bottom (if the depth of the sea was less than 1000 m); some of the CTD casts (approximately every third or fourth) covered the depths from the sea surface down to the sea bottom even if the sea depth exceeded 1000 m.

To estimate the strength of the FSBW or the BSBW or both branches of the Atlantic Water, we applied standard dynamical method. The main problem with geostrophic estimates of velocity from CTD transects lies in the uncertainty of choice of the no motion level (the zero velocity depth). If one expects that the baroclinic current occupies the upper layer or/and some intermediate layer while the deep layer is relatively calm, the no motion level can be chosen somewhere in a supposedly calm deep layer (where the horizontal density gradient is relatively small). On the contrary, in case of a near-bottom gravity flow, one would expect relative stillness

in the overlying layers, so the no motion level can be reasonably chosen somewhere well above the near-bottom flow. The first situation is applicable to the FSBW, which is a near-surface current when entering the Eurasian Basin and is transformed to subsurface, intermediate-layer flow on its pathway along the slope of the Eurasian Basin. The latter situation is applicable to the BSBW in the St. Anna Trough. In view of the above considerations, we adopted for the no motion level either1000 m depth or the sea bottom depth if the latter was smaller than 1000 m for the FSBW, and some level in the vicinity of 50 m depth, where density contours were more or less flat, for the observations of BSBW in the St. Anna Trough (see also below).

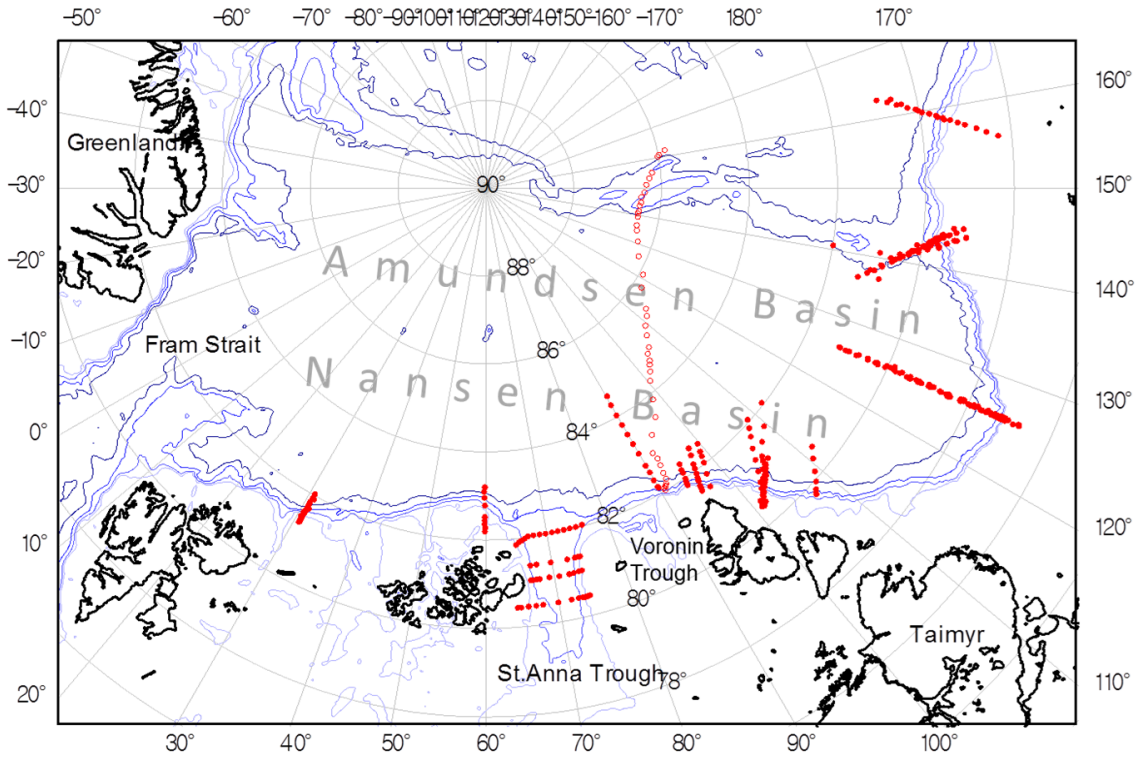

Fig. 1. Bathymetric map of the Eurasian Basin with 300, 500, 1000, and 2000 m contours shown. The red filled and blank circles are the locations of CTD stations on the NABOS and PS96 transects, respectively.

Another problem with the geostrophic estimates of velocity from non-averaged CTD data is caused by vertical undulations of density contours due to internal waves and other ageostophic motions that can cause large fluctuations of horizontal density gradients and, therefore, unrealistically high estimates of geostrophic velocities. However, the effect of ageostrophic motions will almost cancel if we limit ourselves to the geostrophic estimates of volume flow rates.

Since the FSBW brings saline and warm water to the Eurasian Basin, the geostrophic estimates of the volume flow rate were found by integration over the depth range with positive

temperature, $\theta > 0$ °C, and relatively high salinity, $S > 34.5$ (the salinity is given in the practical salinity scale), that is, some areas in the near-surface layer with warm and fresh water (which cannot be attributed to AW) were excluded. For the observations of BSBW in the St. Anna Trough the geostrophic estimates of the volume flow rate were found by integration over a depth range with the non-averaged temperature below 0 °C and the salinity above 34.5. If both branches of AW were present on the transect, the integration was performed over the entire depth range except the cold near-surface layer ($\theta < 0$ °C) and the areas in the near-surface layer with warm ($\theta > 0$ °C) and relatively fresh ($S < 34.5$) water. The zero velocity depth in this case was chosen in accordance to the observed pattern of density contours, i.e. its resemblance with either the near-surface flow pattern or the near-bottom flow pattern (see Section 3 for details). A detailed description of the method for geostrophic estimates of the AW volume flow rate is presented in the paper (Zhurbas, 2019).

3. Results

3.1 Variability of the thermohaline pattern on the AW pathway along the slope of Eurasian Basin

3.1.1 CTD transects analysis

Let us focus on the transformation of thermohaline signatures (i.e. patterns of salinity S, potential temperature θ, and potential density anomaly σ_θ, calculated relative to the atmospheric pressure $p_0 = 0$ dbar, versus cross-slope distance and depth) of the AW flow on its pathway along the slope of the Eurasian Basin. The σ_θ contours on transects at 31°E diverge towards the continental slope margin (to the south), shallowing above the warm/saline core of the AW and sloping down beneath it (Fig. 2), which in terms of geostrophic balance corresponds to the eastward subsurface flow. Such a structural feature of the distribution of isopycnic surfaces was observed on all NABOS transects taken across available continental slope at 31°E. According to Fig. 2 the warm/saline core of the Fram Strait Branch of the AW with the maximum temperature θmax of 4.88°C at the depth $Z_{\theta max}$=102 m and the maximum salinity $Smax$ of 35.11 at the depth Z_{Smax}=176 m is found on the slope at about 1000 m isobath.

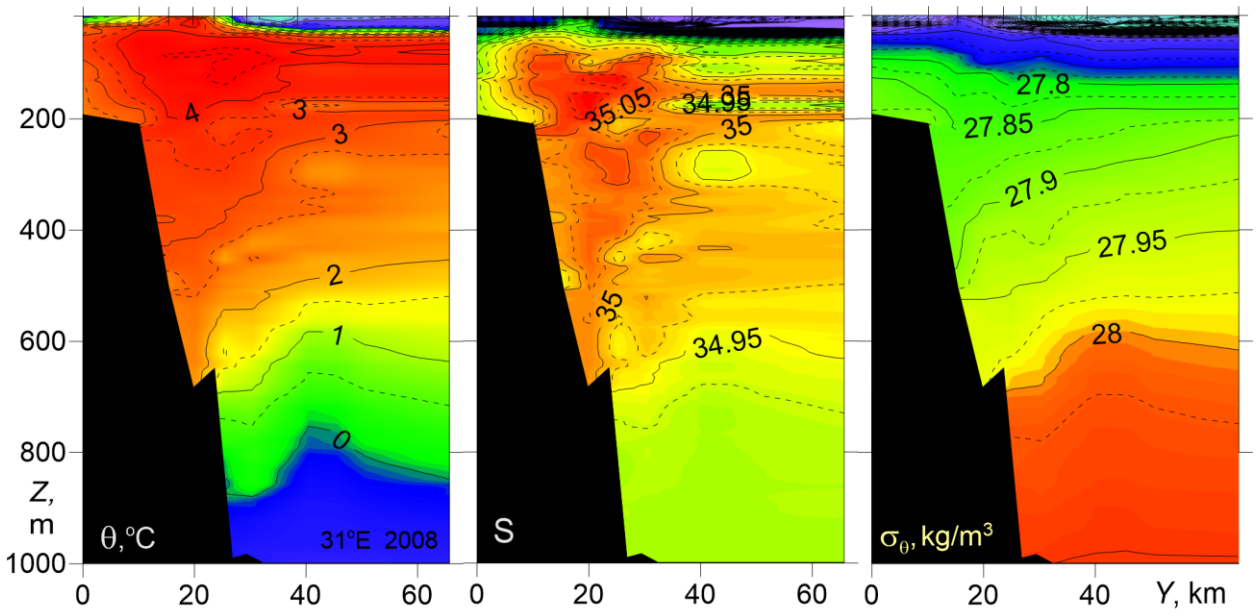

Fig. 2. Temperature θ, salinity S, and potential density anomaly σ_θ versus cross-slope distance and depth for the NABOS-2008 transect across the Eurasian Basin slope at 31°E.

Figure 3 presents temperature, salinity, and potential density versus distance and depth for two zonal transects across the St. Anna Trough at latitudes of 81 and 82°N. A stable pool of cold (θ <0°C) and dense (σ_θ > 28 kg/m^3) water in the bottom layer is seen adjacent to the eastern slope of the Trough. The transfer of the densest water pool to the eastern slope corresponds to a geostrophically balanced near-bottom gravity flow to the North. Note, that the gravity bottom currents are a typical feature of ocean dynamics and can develop in the narrows and troughs of various ocean basins (Arneborg et al., 2007; Zhurbas et al., 2012), so it is natural that the water flowing through St. Anna Trough in the Eurasian basin is transported by a gravity current. It is obvious that in case of near-bottom gravity current the no motion depth level for geostrophic calculations is implied to be well above the current. This near-bottom gravity current carries also waters of Atlantic origin, which are strongly cooled due to mixing with shallow waters of the Arctic shelf seas (the Barents and Kara seas). Above the near-bottom gravity flow of the BSBW one can observe two-core structure of warm FSBW with temperature up to 2.5 °C that enters the St. Anna Trough from the north-west at the western side of the Trough and leaves it for the north-east at the eastern side of the Trough. At 82°N, the BSBW overflows a ridge-like elevation east of the St. Anna Trough (top panels in Fig. 3). Results of studies of the currents velocities and thermohaline characteristics of the waters masses in the St. Anna Trough can be found in (Schauer et al., 2002a, b; Rudels et al., 2014; Dmitrenko et al., 2015).

In order to understand the effect of the FSBW and the BSBW transformation on geostrophic flow rate, it is necessary to identify water masses of different origin. For that purpose the following criterion is often used (Walsh et al., 2007; Pfirman et al., 1994): the water

masses of the FSBW are characterized by $\theta > 0$ °C, and the BSBW can be identified by the following expressions: -2 °C < θ <0 °C, 34.75 < S < 34.95 and 27.8 kg/m^3 < σ_θ < 28.0 kg/m^3. Other approaches to define BSBW are given in (Schauer et al., 1997; Schauer et al., 2002a, b) and (Dmitrenko et al., 2015). According to (Schauer et al., 1997; Schauer et al., 2002a, b) the BSBW includes all waters that enter the Nansen Basin from the St. Anna and Voronin troughs. The temperature of these waters, however, can reach ~1 ºC. The justification for this approach was based on θ-S analysis of the waters of the north-eastern part of the Barents Sea and the St. Anna and Voronin troughs. According to (Dmitrenko et al., 2015), the BSBW consists of two water masses, and the temperature of the warmer water mass can only slightly exceed 0 °C (for more details see section 3.1.2). Here we will rely on the definitions of the FSBW and BSBW proposed in (Dmitrenko et al., 2015).

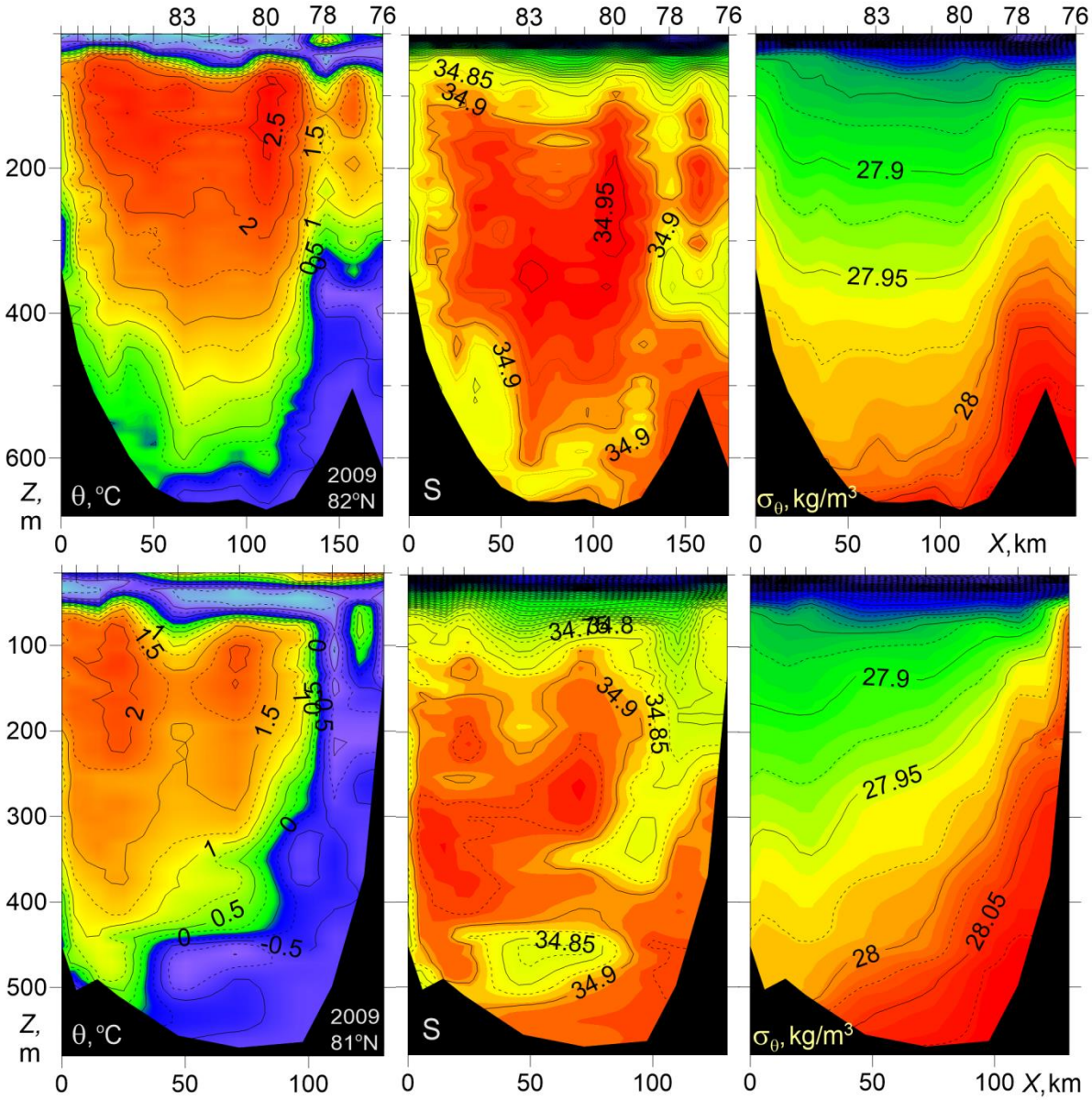

Fig. 3. Temperature θ, salinity S, and potential density anomaly σ_θ versus distance and depth for zonal transects across the St. Anna Trough at latitudes of 81°N (bottom, NABOS-2009), and 82°N (top, NABOS-2009). The X-axis is directed to the east.

In Fig. 4 the CTD transect at 92°E carried out in the *Polarstern*-1996 expedition just east of the entrance point of the BSBW to the Eurasian Basin from the St. Anna Trough and Voronin Trough is presented. It can be assumed that a part of the BSBW extends deep into the Basin, mixing with the FSBW, while another part of the BSBW moves eastward along the slope according to the general cyclonic circulation observed in the Eurasian Basin. On the presented transect the BSBW is observed in the depth range below 600 m as a narrow, about 10 km wide strip of cold water near the slope (see also Subsection 3.1.2) adjacent to a 300 km wide zone occupied by the warm FSBW. The pattern of the potential density of FSBW on this transect is similar to transects at 31°E. Namely, despite of the masking effect of vertical undulations of σ_θ contours caused by internal waves and mesoscale eddies (one of subsurface, intra-pycnocline eddies is probably identified at the distance of Y=510 km), one cannot miss the tendency of shallowing/sloping down the σ_θ contours above/below the FSBW core towards the continental slope margin (to the south) which, in terms of geostrophic balance implies the eastward flow of FSBW. The FSBW core on the 92°E transect is found at 40 km distance from the slope, with the maximum temperature θmax=2.79°C at $Z_{\theta max}$=271 m and salinity $Smax$=34.97 at Z_{Smax}=329 m. Therefore, the FSBW on its pathway along the slope of the Eurasian Basin from 31°E to 92°E has cooled, desalinated, sank and become denser by approx. 2 °C, 0.1, 150 m, and 0.1 kg/m^3, respectively. Another significant feature seen in the PS96 transect is an increased temperature pool in the layer of 180–300 m at the distance of Y=600–750 km in the vicinity of the Lomonosov Ridge which can be attributed to the FSBW return flow cyclonically circulating around the Eurasian Basin (Rudels et al., 1994; Swift et al., 1997). The existence of return flow next to the Lomonosov Ridge is confirmed in terms of geostrophic balance by sloping down density contours towards Y-axis.

According to Schauer et al. (2002 b) where the thermohaline structure along the PS-96 section was studied in detail, the horizontal and vertical scales of the BSBW were taken at 30 km and 800 m, respectively. The difference with our interpretation is due to the fact that we relied on the definition of BSBW as a water mass with a temperature of less than 0 °C.

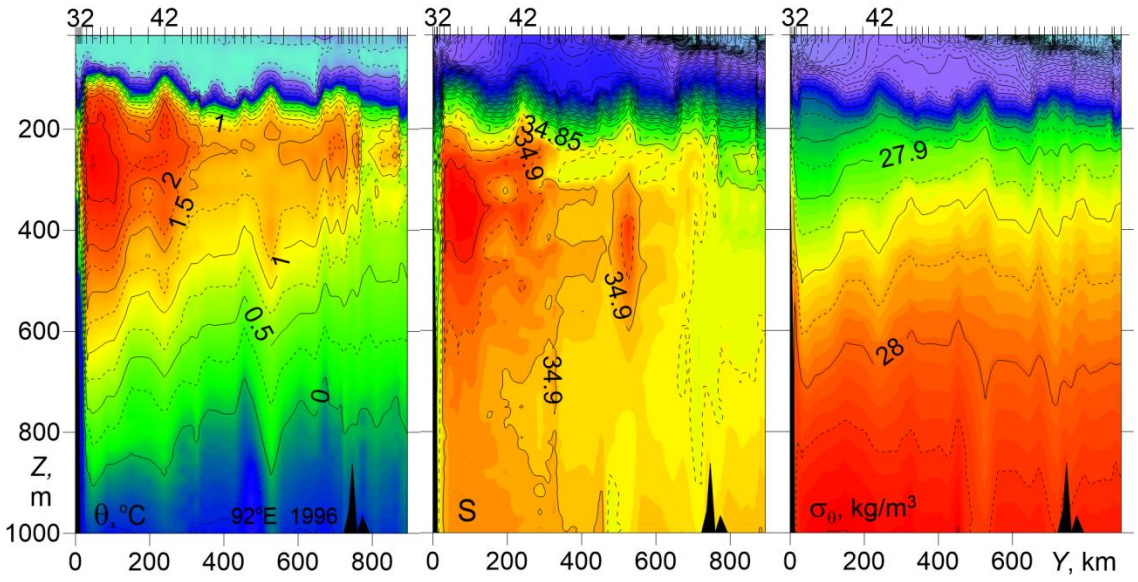

Fig. 4. Temperature θ, salinity S, and potential density anomaly σ_θ versus distance and depth for cross-shelf transects at 92°E (PS-1996).

Further east, in the longitude range of 94–107 °E (NABOS-09), the BSBW being denser dives under the FSBW, and the pattern of potential density on cross-slope transects is characterized by sloping down density contours towards the North in a 150 km wide zone adjacent to the slope (see Fig. 5, top panel) and corresponds to the eastward geostrophic flow provided that the no motion depth level remains within the above-lying layers. Less saline water at the slope is water of the less dense Barents Sea that has entered the Nansen Basin when the slope narrows north of Severnaya Zemlya (Schauer et al., 1997).

The vertical location of the FSBW layer has not changed much relative to the 92°E in the section PS-96 but the maximum temperature has further decreased: in the transect in Fig. 5, the top panel, θmax=1.98 °C at $Z_{\theta max}$=245 m and $Smax$=34.95 at Z_{Smax}=365 m. The bottom panel of Fig. 5 presents the data from transect at 142°E (NABOS-09) which is located on the Lomonosov Ridge, the frontier between the Amundsen and Makarov Basins. The comparison of the two transects obtained in the same year shows that the vertical scale of the especially warm FSBW water (θ>1.5 °C) has significantly decreased. Nevertheless, it is obvious that the FSBW waters are also observed at these latitudes and affect the slopes of isopycnic surfaces in a layer up to 300 m. The cold waters with θ<0 °C, which can be associated with the BSBW, are observed only at two stations in the depth range close to 1000 m, and are practically absent at the depths above 950 m. The slopes of isopycnic surfaces in the bottom panel of Fig. 5 are small, which is typical for weak geostrophic volume flow rate (see Section 3.2). It is worth noting that due to the low variability of the temperature and salinity fields, the water with absolutely stable thermohaline stratification is well visualized (Fig. 5, bottom panel): the temperature decreases and salinity increases with depth. This structural feature of the mean thermohaline stratification is also

common to the Upper Polar Deep Water (UPDW) layer (Rudels et al., 1999; Kuzmina et al., 2011, 2014).

In Fig. 6 three transects are presented, two of which were made at 126°E and 142°E (NABOS-2005) and the third one was made in the Makarov Basin at 159° E (NABOS-2007). On the transect along 126°E large slopes of isopycnic surfaces are observed, which corresponds to a fairly intensive geostrophic flow (see Section 3.2), confined to the depth range of 200−400 m, that is, to the area occupied by the FSBW. At the 142°E transect which is located on the Lomonosov Ridge, the frontier between the Amundsen and Makarov basins, and at the 159°E transect in the Makarov Basin, the FSBW can be still identified as a warm layer within a depth range of 200–400 m, where the maximum temperature has lowered to 1.49 °C and 1.42 °C, respectively (Fig. 6). One can observe some a sloping down of potential density contours towards the continental slope on the 142°E transect implying some eastward geostrophic transport. As to the 159° E transect, one cannot visually identify significant baroclinic flow. In the area of cold waters (the depth range below 800 m) high slopes of isopycnic surfaces are not observed on any sections shown in Fig. 6, which may indicate the weakness or absence of the baroclinic flow.

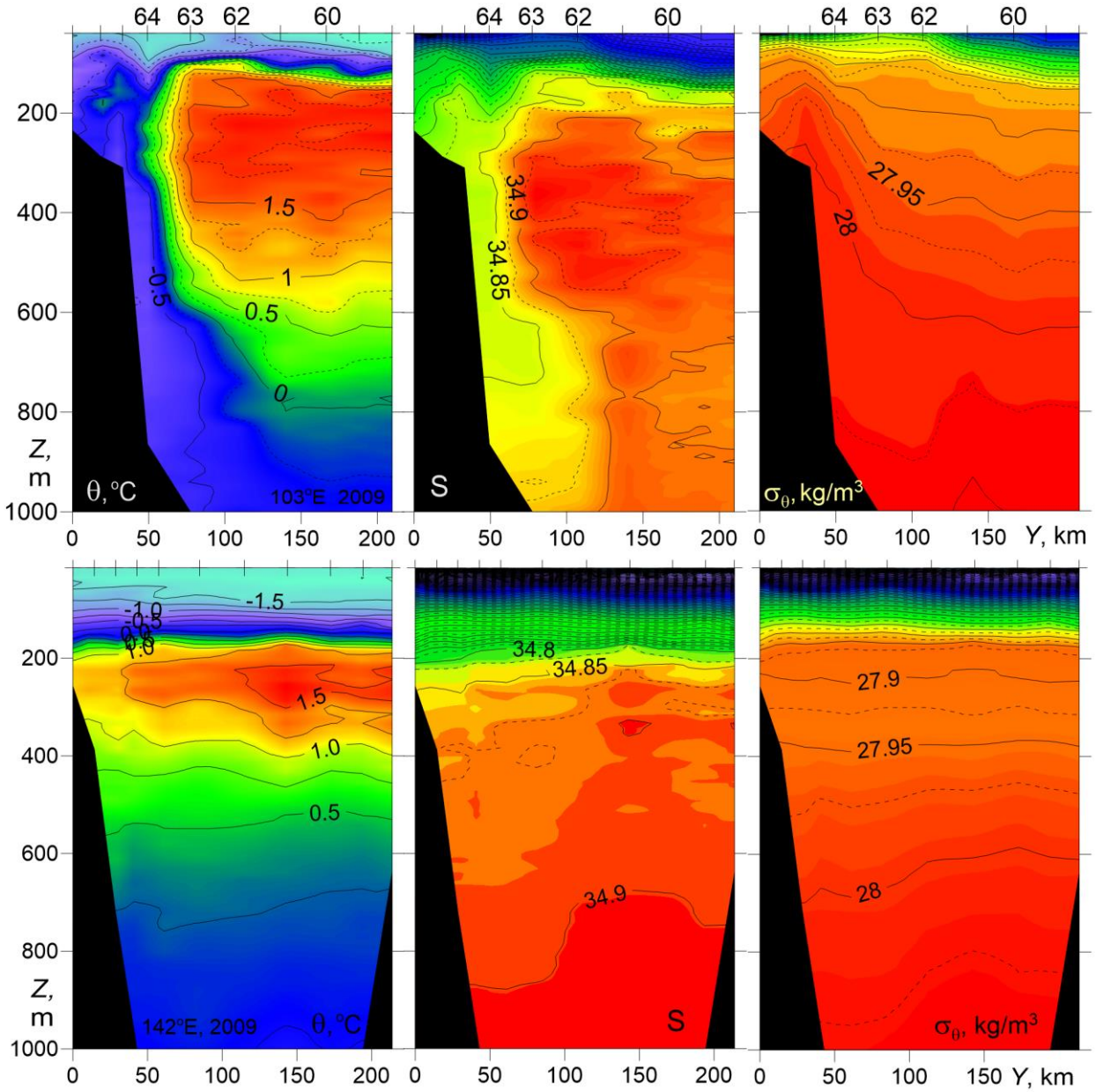

Fig. 5. Temperature θ, salinity S, and potential density anomaly σ_θ versus distance and depth for cross-shelf transects at 103°E (upper) and 142°E (lower) (NABOS-09).

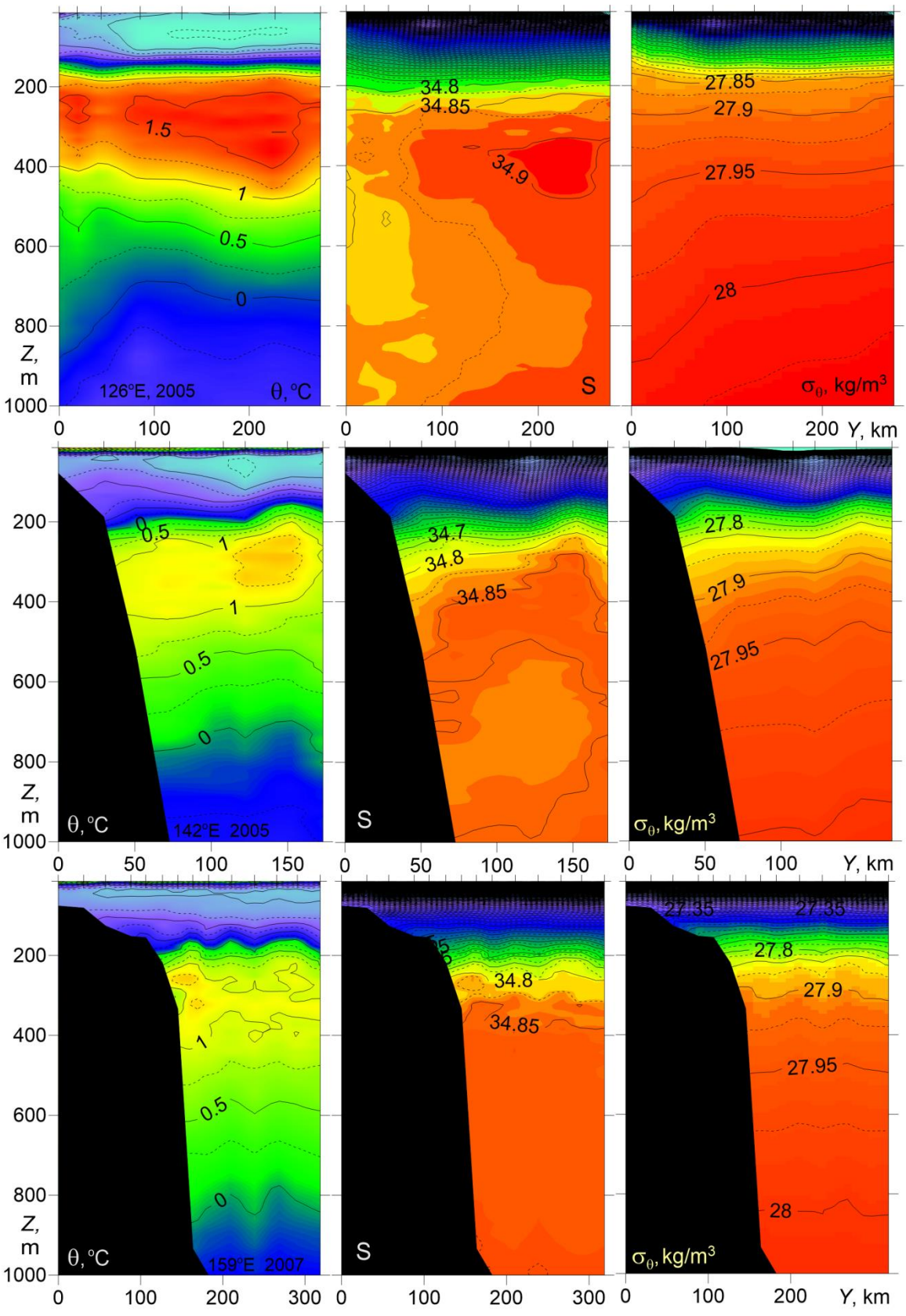

Fig. 6. Temperature θ, salinity S, and potential density anomaly σ_θ versus distance and depth for cross-shelf transects at 126°E, 142°E (top and middle, NABOS-2005) and 159°E (bottom, NABOS-2007).

In summary, the combined FSBW-BSBW structure with isopycnals sloping down to the north (from the slope), is typical for the longitude range 94–107°E. On the transects made along 126°E, 142°E, and 159°E, the slopes of isopycnic surfaces indicating the baroclinic flow, were observed generally in the depth range of 200–400 m, that is in the area occupied by the FSBW. As the FSBW moved along the continental slope of the Eurasian Basin, a significant decrease of temperature was observed in the FSBW core. However, despite this the FSBW was satisfactorily identified at all transects, including the two transects in the Makarov Basin (159°E). The cold waters on the transects along 126°E, 142°E and 159°E, which can be associated with the BSBW, had a minimum temperature above -0.5 °C, were observed in the depth range below 800 m and had a little effect on the spatial structure of isopycnic surfaces and horizontal gradient of density.

3.1.2 *θ-S* analysis

The difficulty in identifying the BSBW in the eastern part of the Nansen Basin is related to the overlapping ranges of temperature and salinity inherent to the BSBW and the UPDW: 0.5 °C<θ<0 °C, and the salinity is close to 34.9 (Rudels et al., 1994; Walsh et al., 2007). It is also important to note that the BSBW in the St. Anna Trough mixes with the FSBW. Therefore, not only the cold Atlantic Waters, which are transported by the bottom gravity current, but also mixed warmer waters can enter the Nansen Basin through the Trough (see Fig. 3). It is expected that a detailed *θ-S* analysis of different CTD sections can provide useful information on the transport and transformation of FSBW and BSBW. Note that a pronounced *θ-S* signal clearly indicates that the water mass has entered the area of observation. The absence of a signal indicates one of the following: a) the water mass did not enter the area of observation; b) it entered the area of observation being highly transformed, namely, mixed with other waters.

The differences in the behavior of the *θ-S* values are observed in the upper and deep layers of the Eurasian Basin and the St. Anna Trough (Fig.7). On the other hand, one cannot miss a similarity in the shape of the *θ-S* curves in the salinity range of 34.5−35.0. The similarity is obviously caused by the presence of FSBW. The plots in Fig. 7 demonstrate the transformation of the FSBW and BSBW moving along the continental slope of the Eurasian Basin. More detailed information on the BSBW transformation can be extracted from *θ-S* diagrams presented in Fig. 8.

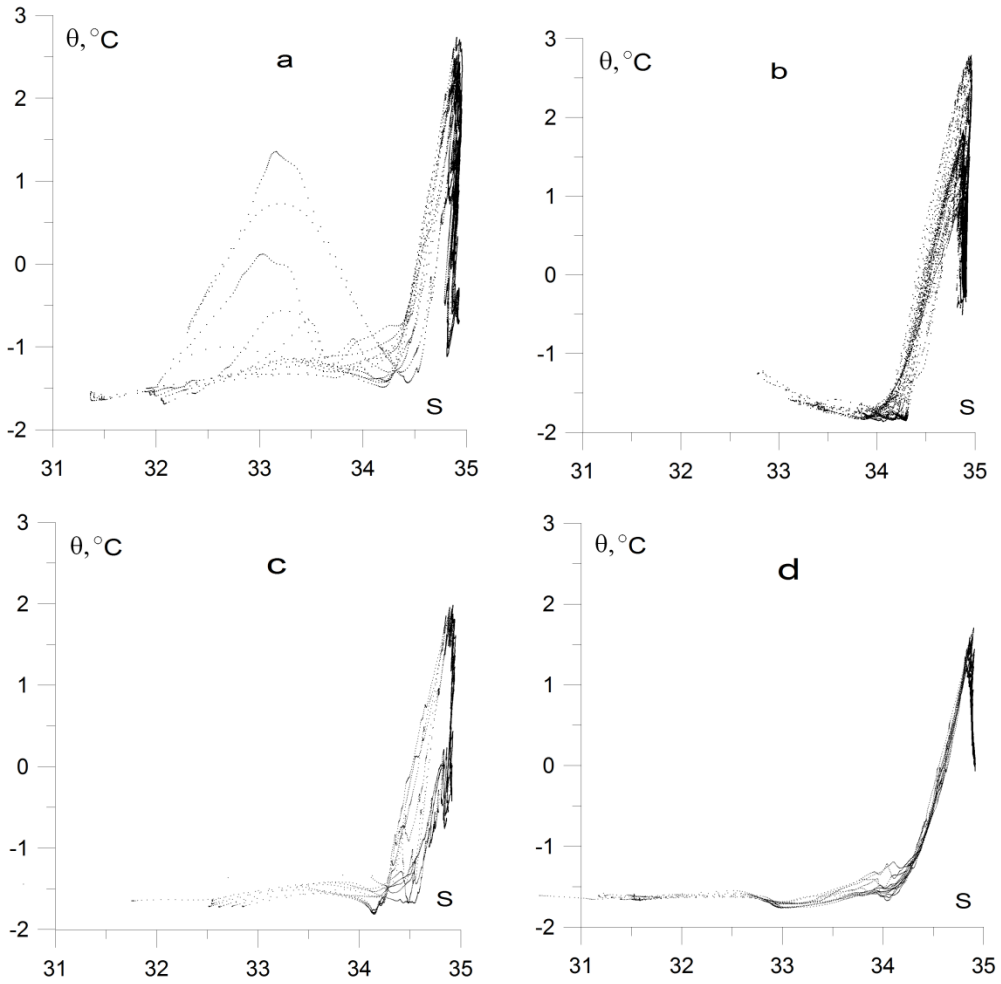

295 Fig. 7. *θ-S* diagrams based on the CTD profiling in (a) the St. Anna and Voronin troughs (NABOS-09, 82° N), (b) the PS-96 section at 92°E, and the NABOS-09 sections at 103°E (c) and 142°E (d). For convenience of presentation, the points of the *θ-S* curves with salinity below 30 were dropped.

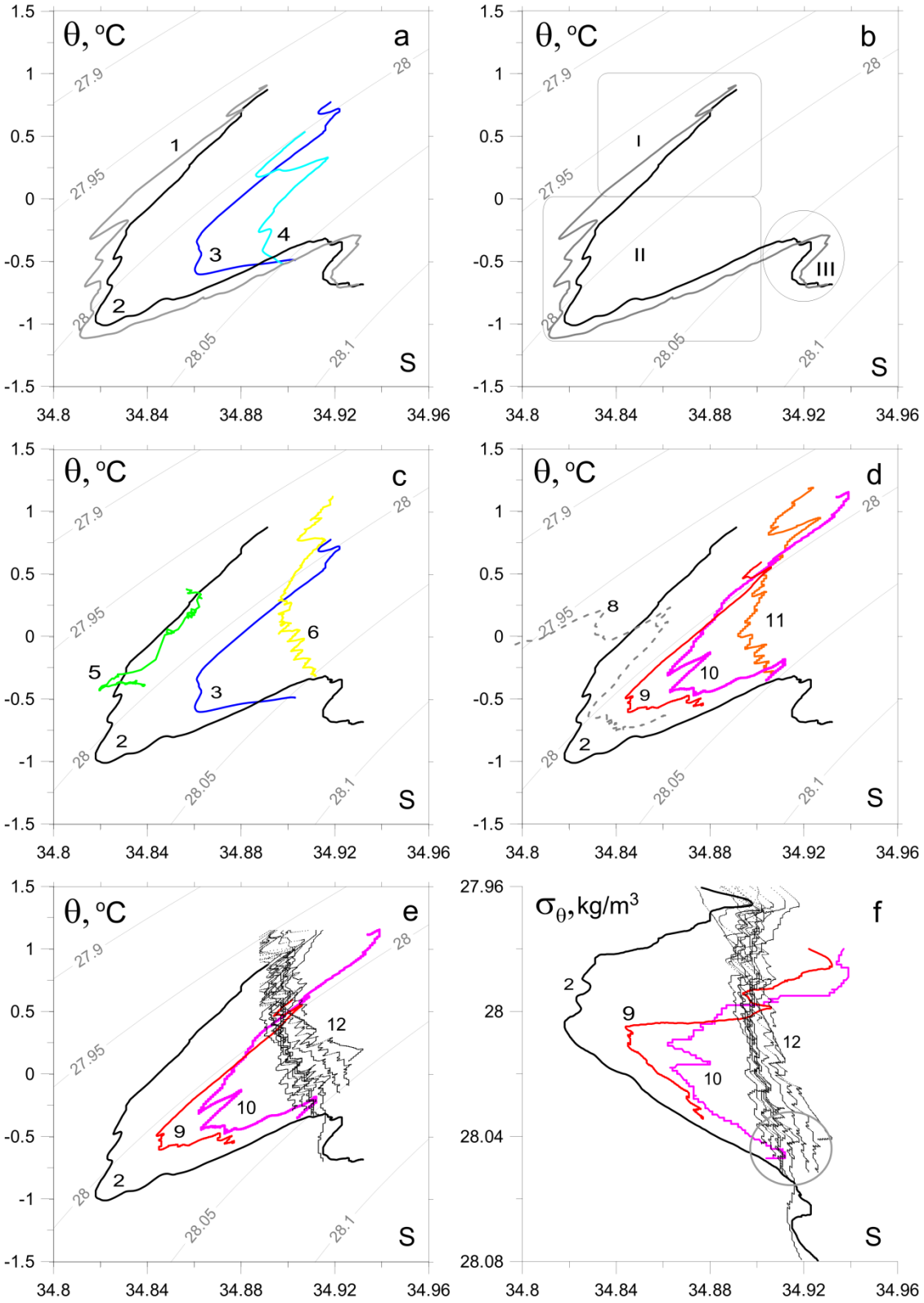

300 Fig. 8. Thermohaline ~~indexes~~ values of the BSBW and FSBW: a) based upon the CTD profiles, obtained in the St. Anna Trough (NABOS-09, section 82°N), curves 1−4 correspond to the stations (st.) 76, 78, 83 and 80, respectively; b) the same as "a" but only curves 1 and 2 are presented; regions I, II, III illustrate three different water masses in accordance with (Dmitrenko et al., 2015); for explanation see the text; c) based upon the section of PS-96, curves 5 and 6
305 corresponding to st. 32 and 42, respectively (depth range 600−1000 m), curves 2 and 3 are

shown for the reference; d) for CTD profiles at the 103°E section, NABOS-09, curve 8 (st. 64), curve 9 (st. 63), curve 10 (st. 62), curve 11 (st. 60), and curve 2 for the reference (see Fig. 5 for the location of the stations); e) based upon the CTD profiles in the depth range 500−1200 m measured at the 126°E (section of NABOS-09), curves 12; curves 2, 9 and 10 are shown for the reference; f) the same as "e" but presented in coordinates σ_θ, S.

The θ-S curves marked as 1 and 2 in Fig.8a correspond to stations 76 and 78, respectively, which were located at the eastern slope of the St. Anna Trough just in the near-bottom gravity current carrying the BSBW, while the curves marked as 3 and 4 correspond to stations 83 and 80 located near the mid-point (thalweg) of the Trough in the western periphery of the gravity current (the location of the stations is shown in Fig. 3). To visualize better the BSBW transformation, the points of θ-S curves in the temperature and salinity ranges of $\theta > 1.2$ °C and $S < 34.76$, respectively, were omitted. The same kind of similarity of the θ-S curves in the St. Anna Trough was observed within NABOS Program in other years (NABOS-13, NABOS-15).

The curves 1 and 2 in Fig. 8a have similar knee-like shape (Dmitrenko et al., 2015) formed by (i) the upper warm and saline water layer of the FSBW ($\theta >> 0$ °C), (ii) the intermediate colder and fresher water layer of BSBW ($\theta < 0$ °C) underlying the FSBW, and (iii) the denser more warmer and saltier "true" mode of the BSBW ($\theta \approx 0$ °C), see Fig. 8b: FSBW (region I), BSBW (region II), "true" mode BSBW (region III). The difference between the BSBW and "true" BSBW is in that the former is more diluted with the colder and fresher Barents Sea water (see paper by Dmitrenko et al. (2015) for more details). We will be interested in the transformation of the main part of the knee (region II), namely the transformation of the moving along the slope BSBW.

In Fig. 8c the comparison of typical θ-S curves related to the St. Anna Trough (they are also shown in the other panels of Fig. 8 for reference) with that of the 92°E section of PS-96 is given: the curves 5 and 6 correspond to st. 32 and st. 42 (depth range 600−1000 m) of the PS-96 section, respectively. St. 32 was located next to the slope, while st. 42 was located about 250 km apart from the slope. The coincidence of curve 5 with a part of curve 2 evidences for the BSBW moving along the slope of Nansen Basin (see Fig. 4 and its legend 1). Curve 6 corresponds to the UPDW. The θ-S diagrams for CTD profiles at the section 103°E are presented by curves 8-11 (see Fig. 5 for the locations of stations). Curves 8, 9, and 10 are similar to curve 2, and indicate the BSBW being an along-slope flow. Curve 11, being similar to curve 6 in Fig. 8c, corresponds to the θ-S values of the UPDW. However, the BSBW is not observed in the section 126°E: see Fig. 8e, where a collection of θ-S curves (collectively referred as 12) presents all CTD profiles in the depth range 500−1800 m measured at the section 126°E of NABOS-09. Also we do not

observe the BSBW further to the east on the section 142°E of NABOS-09 (not shown) as well as in the Makarov Basin.

To estimate the potential density of deep waters at the sections 103°E and 126°E σ_θ-S diagrams are shown in Fig. 8f: curves 2, 9 and 10 correspond to θ-S curves 2, 9 and 10 presented in Fig. 8d, curves 12 correspond to curves 12 in Fig. 8e. As one can see, the BSBW is characterized by knee-shape diagram also in coordinates σ_θ, S. However the knee-shape diagram is not observed along 126°E in these coordinates. The dense and cold deep waters in the section 126°E have σ_θ, θ, S values typical for the "true" BSBW mode (Dmitrenko et al. (2015)). Nevertheless, it is hardly correct to consider these waters (see σ_θ, S values inside the circle; Fig. 8f) as the true BSBW mode, since σ_θ, θ, S values of these waters satisfactorily correspond to σ_θ, θ, S values of the UPDW in the western part of the Nansen Basin (at longitudes to the west of 90°E). To evaluate the transformation of the "true" mode of the moving along the slope BSBW an additional analysis is required, which is beyond the scope of this paper.

The results presented in Fig. 8 show that the BSBW signal which is characterized by the knee-shape diagram in coordinates θ-S and σ_θ-S, is not visible at 126°E. This is consistent with the conclusion formulated in Subsection 3.1.1 that by 126°E the BSBW is not accompanied by any noticeable perturbations of isopycnals. Moreover, given the characteristic feature of the θ-S structure of BSBW in the St. Anna Trough (curves 1−4 in Fig. 8a) was observed in other years, we carried out a similar analysis using all available CTD data and found that the BSBW signal is either strongly weakened or not visible at this longitude (see Fig.9). The only exception was 2002, when the knee was still observed. It suggests that the BSBW and FSBW begin to mix intensively immediately after 103ºE. However, the FSBW signal is well identified at 126ºE and further along the slope of the Eurasian Basin (and even in the Makarov Basin), while we cannot say the same about the BSBW signal. Thus, one may assume that east of 126ºE the geostrophic volume flow rate of the AW is determined mainly by the FSBW.

According to (Schauer et al., 1997), the FSBW and BSBW merge and mix around 126°E and then spread along the slope as a single flow. The absence, as a rule, of the BSBW signal at 126°E and further to the east along the slope can be considered a kind of phenomenon: if such a situation is typical for the dynamics of the Eurasian Basin, then the answer to the question − why is there a strong relaxation of this signal to 126°E − is important for understanding the transformation and mixing of the BSBW.

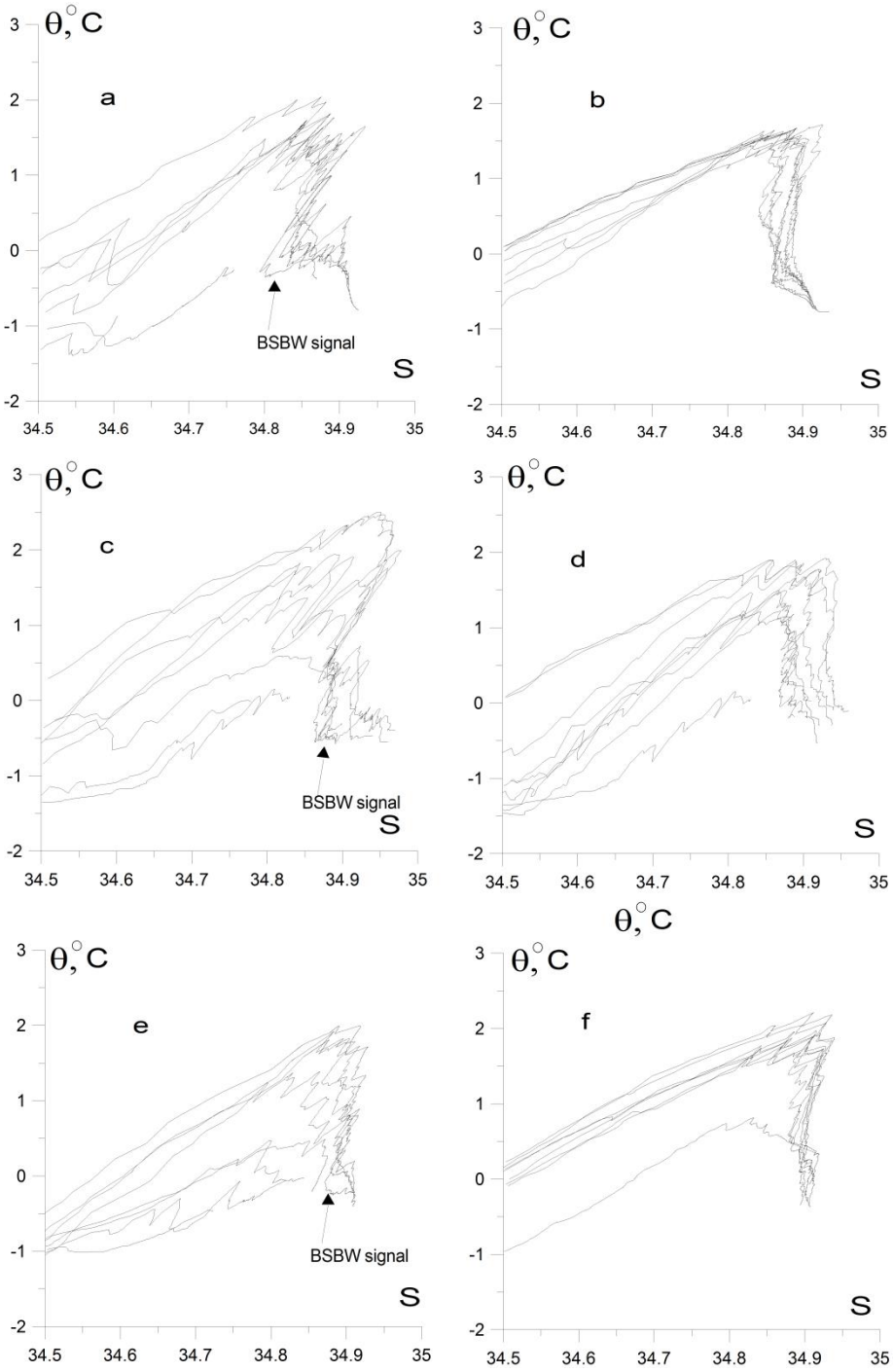

Fig. 9. *θ-S* diagrams based on the CTD profiling : NABOS-05: (a) and (b), 103°E (a), 126°E (b); NABOS-06: (c) and (d), 103°E (c), 126°E (d); NABOS-08: (e) and (f), 103°E (e), 126°E (f).

3.2 Characteristics of the Atlantic Water flow and geostrophic estimates of the volume flow rate

The estimates of *V*, as well as estimates of the hydrological parameters describing the AW flow in the Eurasian and Makarov Basins, are presented in Table 1. The geostrophic estimates of the near-bottom gravity volume flow rate of the BSBW in zonal transects across the St. Anna Trough are presented in Table 2. The only exception is the transect at 82°N where the near-

bottom gravity current is seen to have a considerable eastward component due to overflow across a sufficiently deep ridge (approx. 500 m deep) east of the St. Anna Trough (Fig. 3, top panels). The probable presence of the eastward constituent of indefinite value makes questionable the results of geostrophic calculations only accounting for the northward constituent of the flow. Note also that prior to the BSBW entering the area of the Eurasian Basin, our estimates refer to the FSBW; to east of this region our estimates should be attributed to the joint contribution of two branches – the FSBW and BSBW – to the transfer of the AW.

The hydrological parameters shown in Table 1 can be interpreted as follows. The maximum water temperature of the AW may exceed 5 °C in cases when the AW inflow to the Eurasian Basin consists of especially warm water masses. A typical change in the maximum temperature of the moving along the continental slope AW over a distance of about 1000 km is approximately 1–2 °C. A typical change of the maximum salinity of the moving along the slope AW over the same distance does not exceed 0.1. Such values of the maximum temperature of the AW lead to a slight increase in potential density and therefore a deviation of the AW from the isopycnic distribution should be expected. This effect is most likely associated with the exchange of heat, salt, and mass with the surrounding waters due to the formation of intrusive layering and the influence of double diffusion (on the observation and study of intrusions in the Arctic Basin see, e.g., Rudels et al., 1999; Kuzmina et al., 2011; Polyakov et al., 2012; Kuzmina et al., 2013) and also with the AW core transformation by sea ice melting and cooling (Rudels, 1998). The intrusions, in particular, can also contribute to the reduction of the AW heat and salt content and the volume flow rate. The differences in the AW heat and salt content and the volume flow rate can be clearly seen from the PS-96 section when comparing data from stations near the continental slope of the Eurasian Basin at 92°E and from the vicinity of the Lomonosov Ridge at 140°E.

It is worth noting that the maximum value of the AW temperature (θ_{max}) according to the presented data is always observed in the upper layer of the Eurasian Basin at the depths below the density jump layer but not exceeding 350 m, while the maximum salinity (S_{max}) at sections in the eastern part of the Basin can be observed at depths greater than 1000 m.

$X_{\theta max}$ in Table 1 is the distance of the AW core (which can be associated with θ_{max}) from the slope/shelf boundary. The highest value and the maximum variation of this parameter is observed near 126°E and 142°E, where two-core structure of AW often observed (Pnyushkov et al., 2015).

A striking feature of the data is a noticeable increase of θ_{max} in 2006 at 31°E and 103°E. This intensive warming of the AW was first reported in (Polyakov et. al., 2011). The present

results show that the increase of the temperature of the AW in 2006 was also accompanied by an increase of volume flow rate of the geostrophic current (see Table 1, the volume flow rate at the section along 103°E, and reasonings below). This can be caused not only by the warming of the AW, but also by an increased inflow of the AW to the Eurasian Basin.

As it can be seen from Table 1, the evaluations of geostrophic current transport in the range of 31–159°E are characterized by a high variability. This may be due to the following reasons: a) the deviation of some sections from the normal to the current; b) the difference in the horizontal scales of the sections; c) some uncertainty in the choice of the reference level for geostrophic calculations; d) meandering of the flow; e) the effect of synoptic quasi-geostrophic eddies on the flow volume rate. All of these reasons contribute some noise to the resulting volume flow rate estimates. In order to find statistically consistent estimates of the variability of geostrophic volume flow rate along the slope of the basin based on a limited material, the following was done. The volume flow rates obtained for all sections within the range 31º–92 ºE for different years were used to calculate the mean volume flow rate (region I; the number of volume flow rate values to be averaged is $N = 6$). Similarly, the average volume flow rate was calculated for the region 94º–107ºE (region II; $N = 9$). The remaining average estimates of geostrophic volume flow rate were calculated for sections 126ºE (region III; $N = 9$), 142ºE (region IV; $N = 10$) and 159ºE (region V; $N = 2$). Then the confidence intervals with a probability of 95% (typical confidence interval) and 80% (acceptable confidence interval for working with a limited statistical material) were determined using the Student t-distribution. All estimates of average volume flow rates and confidence intervals are presented in Tables 1 and 2.

The above mean estimates allow us to conclude that the volume flow rate increases from region I to region II, then decreases to region III and after that decreases to region IV, followed by a sharp decrease in region V. However, the 95% confidence intervals vadidate only the differences between the mean volume flow rate in region II and the values in regions IV and V. Confidence intervals for regions II, IV and V are (0.46; 1.72), (0.12; 0.44) and (-0.37; 0.43), respectevely. These intervals indicate that the mean volume flow rate in region II exceeds the value of the same parameter in regions IV and V with a high probability of 95%. The 80% confidence intervals overlap only for regions III and IV, (0.25; 0.53) and (0.18; 0.38), respectively. In this regard, we can declare that the above described change in the volume flow rate along the slope is reliable with a probability of 80%, except for changes in volume flow rate from region III to region IV.

The above values of the mean volume flow rate and confidence intervals also suggest that the increase in volume flow rate in 2006 was caused by the climate impact, and not by the

"noise" in the data. Indeed, the volume flow rates in regions II, III, and IV in 2006 exceeded the upper limits of the corresponding 95% confidence intervals. From statistical point of view such a significant increase in volume flow rates at the same time in three sections is a very rare event that can hardly be explained by random "noise" in the data caused, for example, by the influence of synoptic eddies.

Let us turn our attention to the following features of the volume flow rate estimates: high volume flow rate estimates at 96°E, 103°E, 107°E, a negative volume flow rate estimate at 126°E in 2013 and low volume flow rate estimates at 31°E, 98°E in 2009 (Table 1). Indeed, the AW volume flow rate in the BSBW area of entry into the Eurasian Basin in 2013 was almost equal to the maximum volume flow rate in 2006 (103°E) and was quite high up to the longitude 107°E. This phenomenon as well as the intense warming in 2006 can be associated with the impact of climate conditions. The negative volume flow rate at 126°E was, according to the authors, due to the influence of local return flows which can be observed near the slope (Pnyushkov et al., 2015). Low FSBW volume flow rate estimates in 2009 are probably associated with a strong deviation of the flow from the slope, which may have been resulted in an underestimation of the AW volume flow rates due to the small length of the cuts to the north (see also below).

It is important to analyze average values of volume flow rate V_{mean} in region I and in the St. Anna Trough. The mean values of the FSBW volume flow rate is $V_{mean} = 0.5$ Sv This estimate of volume flow rate is about half the estimate of the BSBW mean volume flow rate, $V_{mean} = 0.79$ Sv for $N = 3$ (see Table 2). (The 80% confidence intervals do not overlap indicating that the BSBW volume flow rate does exceed the FSBW volume flow rate). The BSBW mean volume flow rate exceeding nearly twice the FSBW mean volume flow rate results in a dominance of the BSBW pattern of potential density contours in the longitude range of 94–107°E (область II), where the both branches of the AW are present. Moreover, the sum of the mean values of the FSBW and the BSBW volume flow rate geostrophic estimates, $V_{mean} = (0.5+0.79)\ 10^6 = 1.29$ Sv, corresponds well to the mean geostrophic estimate of volume flow rate for the combined FSBW and BSBW flow within the region II: $V_{mean} = 1.09$ Sv. Thus, the increase in geostrophic volume flow rate in region II is mainly due to the influence of the BSBW. It should be noted that, according to sections 3.1.1 and 3.1.2, the decrease in geostrophic volume flow rate in region III can also be associated primarily with the BSBW, namely, with the decrease in the BSBW signal in 126ºE section and further along the slope.

Finally, at the section 159°E located in the Makarov Basin, the geostrophic estimate of the along-slope volume flow rate of mixed waters of the FSBW and the BSBW has further greatly reduced down to V_{mean} =0.03 Sv for N =2, which is of more than one order of magnitude smaller than that in the Nansen and Amundsen Basins. Despite the low statistical significance of the latter estimate (due to small value of $N=2$) one may conclude that the major part of the AW entering the Arctic Ocean circulates cyclonically within the Nansen and Amundsen Basins, and only its small part flows to the Makarov Basin (Rudels et al., 2015; Rudels, 2015). However, additional studies using more CTD data are required to confirm this result.

Table 1. Characteristics of the Atlantic Water flow in the course of its propagation along continental slope of the Eurasian Basin of the Arctic Ocean. *Dist* is the along-slope distance from the Fram Strait; θ_{max} is the maximum temperature; $\sigma_\theta(Z_{\theta max})$, $S(Z_{\theta max})$, $Z_{\theta max}$, and $X_{\theta max}$ are the values of potential density, salinity, depth, and lateral displacement from the slope for the point θ_{max}; S_{max} and Z_{Smax} are the same as θ_{max} and $Z_{\theta max}$ but for the salinity; V is the geostrophic estimate of the volume flow rate. The mean values and 95% / 80% confidence intervals of the volume rate, V_{mean}, calculated separately for CTD transects at 31−92°E, 94−107°E, 126°E, 142°E and 159°E, are presented too. The last row in the Table presents the characteristics of the return flow of the AW by the Lomonosov Rigde at the longitude 140°E and latitude 86.5°N (PS96, see Fig. 1). Year is given in the first column (e.g. NABOS06 corresponds to 2006).

Exp	*Lon* [°E]	*Dist* [km]	θmax [°C]	$\sigma_\Theta(Z_{\theta max})$ [kg/m^3]	$S(Z_{\theta max})$	$Z_{\theta max}$ [m]	$X_{\theta max}$ [km]	S_{max}	Z_{Smax} [m]	V [Sv]
NABOS06	31	404	5.670	27.579	34.980	42	-11	35.099	72	0.57
NABOS08	31	404	4.883	27.771	35.103	101	0	35.105	176	0.80
NABOS09	31	404	3.691	27.818	34.999	89	0	35.002	91	0.10
NABOS09	60	856	2.503	27.891	34.951	175	10	34.981	363	0.47
NABOS13	90	1290	2.600	27.903	34.975	250	41	34.996	333	0.46
PS96	92	1322	2.786	27.875	34.960	271	33	34.968	329	0.58
										V_{mean} = 0.50 ±0.24 / ±0.14 Sv
NABOS15	94	1355	2.445	27.946	35.012	331	33	35.015	365	0.47
NABOS13	96	1388	2.548	27.902	34.969	207	70	34.978	264	2.06
NABOS09	98	1421	2.300	27.906	34.948	220	79	34.971	345	0.09
NABOS05	103	1561	2.029	27.870	34.876	179	39	34.934	309	0.32
NABOS06	103	1561	2.528	27.888	34.950	220	50	34,978	260	2.23
NABOS08	103	1561	1.980	27.886	34.891	201	60	34.929	325	0.42
NABOS09	103	1561	1.984	27.913	34.925	244	50	34.951	365	0.87
NABOS13	103	1561	2.278	27.904	34.942	215	80	34.956	419	1.59
NABOS13	107	1695	1.903	27.937	34.945	359	120	34.948	404	1.77
										V_{mean} = 1.09 ±0.63 / ±0.38 Sv
NABOS02	126	2104	1.406	27.938	34.902	324	243	34.932	2061	0.05
NABOS03	126	2102	1.341	27.941	34.899	336	342	34.921	1886	0.41
NABOS04	126	2102	1.770	27.906	34.896	271	87	34.925	2431	0.61
NABOS05	126	2102	1.695	27.936	34.926	359	227	34.935	2841	0.75
NABOS06	126	2102	1.905	27.923	34.930	284	193	34.960	968	0.77
NABOS07	126	2102	2.085	27.907	34.928	266	242	34.942	340	0.60
NABOS08	126	2102	2.195	27.885	34.911	206	235	34.939	365	0.31
NABOS09	126	2102	1.907	27.909	34.913	316	33	34.932	1018	0.40
NABOS13	126	2102	1.946	27.937	34.949	346	228	34.951	428	-0.21

NABOS15	126	2102	1.653	27.918	34.898	246	400	34.942	3816	0.22
										V_{mean} = 0.39 ±0.22 / ±0.14 Sv
NABOS03	142	2456	1.089	27.912	34.841	269	41	34.862	1000	0.06
NABOS04	142	2456	1.401	27.909	34.865	281	0	34.907	1608	0.21
NABOS05	142	2456	1.492	27.906	34.870	284	100	34.906	1550	0.26
NABOS06	142	2456	1.981	27.874	34.876	234	111	34.960	1016	0.60
NABOS07	142	2456	1.855	27.879	34.870	231	0	34.920	2064	0.09
NABOS08	142	2456	1.599	27.915	34.890	260	200	34.908	347	0.23
NABOS09	142	2456	1.704	27.915	34.900	253	101	34.917	1082	0.22
NABOS13	142	2456	1.475	27.940	34.909	331	115	34.926	1150	0.18
NABOS15	142	2456	1.353	27.936	34.892	326	106	34.913	1372	0.63
										V_{mean} = 0.28 ±0.16 / ±0.10 Sv
NABOS07	159	2783	1.424	27.887	34.839	255	0	34.880	1075	-0.01
NABOS08	159	2783	1.383	27.893	34.843	245	0	34.889	1266	0.06
										V_{mean} = 0.03 ±0.40 / ±0.10 Sv
PS96back	140E 86.5N	3178	1.812	27.890	34.880	219	≈ 700	34.902	472	-0.09

Table 2. Geostrophic estimates of the volume flow rate for near-bottom gravity flow of the Barents Sea Branch of Atlantic Water (BSBW) on zonal transects across the St. Anna Trough.

Exp	NABOS09	NABOS13	NABOS15	
Lat [°N]	81.00	81.33	81.41	V_{mean}
V [Sv]	0.89	0.73	0.76	0.79 ±0.22 / ±0.10

3.3 Interannual variability of the AW temperature-salinity values and the volume flow rate

Within the NABOS project, in accordance with Table 1, the cross-slope CTD transects at 103°E, 126°E, and 142°E were repeatedly performed for a number of annual campaigns: 2005, 2006, 2008 and 2013 (103°E), 2002–2009, 2013 and 2015 (126°E), 2003–2009, 2013, and 2015 (142°E). The repeated transects may contain some information on inter-annual variability of the AW, and we attempted to explore such a possibility.

Time series of the maximum temperature of the AW, θ_{max} , and the related values of salinity $S(\theta_{max})$ and potential density anomaly $\sigma_\theta(\theta_{max})$ (Fig. 10) show that the period of 2006–2008 was characterized by not only an increased temperature of the AW in the eastern part of the Eurasian Basin but an increased salinity and density reduction. The temperature excess during this period was as large as about 0.6–1.0 °C relative to the years 2002–2003 and 0.3–0.6 °C relative to the years 2013–2015. The time series of corresponding values of salinity $S(\theta_{max})$ displayed in 2006 local maxima at the transects 126°E and 142°E, and the absolute maximum at the transect 103°E; the salinity excess for the maxima largely decreased with the longitude from approximately 0.06 at 103°E to less than 0.01 at 142°E. In accordance with our analysis the time

series of θ_{max} had a maximum in 2013 but only at 103°E (see Table 1 and Fig.10). The time series of $S(\theta_{max})$ display an increase of AW salinity in 2006–2008 and 2013 also, that can be referred to as a AW salinization in early 2000s. The change of salinity of AW at 142°E in time also draws attention to the following aspect: the salinity increases almost monotonously in the period from 2003 to 2013. How can such behavior of salinity be explained is not clear. It is also worth noting that the maxima of θ_{max} and $S(\theta_{max})$ in 2006 and 2013 (at 103°E) were accompanied by the volume flow rate highs.

4 Discussion

Here we will discuss the following three issues: a) differences in the identification of the BSBW; b) comparison of the geostrophic volume flow rate estimates obtained in this work with the other studies; c) the reasons for the weakening of the BSBW signal at 126 ºE and further east.

a) Advection and interaction of waters with different θ-S characteristics in the Arctic Basin, as well as the impact of climate change that has been observed over the past decade (Polyakov et al., 2017) complicate the accurate identification of water masses. However, a robust approach to the determination of the FSBW and BSBW, which was proposed in (Dmitrenko et al., 2015), is effective for distinguishing the water masses of these AW branches. As an exception, this approach does not take into account some cases, namely when the FSBW temperature is below 0 °C (see Fig. 2 in (Dmitrenko et al., 2015)), and/or the BSBW temperature is close to 1 °C (see Fig. 6 in (Schauer et al., 2002a)). If such cases are rare, then either of the two approaches can be used to identify the BSBW and FSBW. Indeed, the identification of the BSBW on the PS-96 section in our case (we used the approach of (Dmitrenko et al., 2015; see paragraph 3.1.1)) does not differ much from that of (Schauer et al., 2002b). However, these discrepancies can lead to almost an order of magnitude difference in estimates of the volume flow rate of the BSBW only due to the differences in the BSBW cross-sectional area.

b) Based on the velocity measurements with moored instruments (1997−2010) in the area of the West Spitsbergen Current (WSC) near the Fram Strait (zonal transect at ~78º50′ N), it was found that approximately 3 Sv of the AW flow into the Nansen Basin (Beszczynska-Möller et. al., 2012). The long-term mean volume transport confined to the WSC core branch (or Svalbard branch in accordance with (Schauer et al., 2004)) included 1.3±0.1 Sv of the AW warmer than 2ºC. The offshore WSC branch (or Yermak branch) carried on average 1.7±0.1 Sv of the AW. Investigation of water transport in and north of the Fraim Strait based upon CTD-measurements on zonal and meridional sections have been done by Marnela et al (2013). The variability range of the estimates of the AW geostrophic transport of the Svalbard branch was calculated for

meridional sections made in 1997, 2001, and 2003 (summer/fall), and was between 0.06 Sv and 0.7 Sv. In the paper (Kolås and Fer, 2018) observations of the oceanic current and thermohaline field (summer in 2015) in the three sections were used to characterize the evolution of the WSC along 170 km downstream distance. Geostrophic transports were calculated on the basis of absolute geostrophic velocities and it was shown that from 0.6 Sv to 1.3 Sv of the AW is carried by the Svalbard branch. In accordance with earlier studies of the currents in the Fram Strait, recirculation of the AW can be significant, and the volume flow rate of the AW entering the Arctic Ocean can be equal only 1 Sv (Rudels, 1987), or it ranges from 0.6 Sv to 1.5 Sv (Aagaard and Carmack, 1989).

Our estimate of the mean volume flow rate V_{mean} in region I (31º−92 ºE) is in the range of variation in the above estimates. However, the upper confidence limit of our estimate does not reach 1 Sv. Moreover, we used the inequality T> 0ºC to identify the AW while in (Beszczynska-Möller et al., 2012) the volume flow rates of the AW entering the Eurasian Basin through the Fram Strait were determined from the T > 2 °C condition. In this regard, we can admit that our assessment in region I is somewhat underestimated. Probably, this may be due to the fact that the sections along the longitudes 31°E (see Fig. 1) are less than 100 km. Actually, at the sections along this longitude (Fig. 2, upper panel) only a part of the FSBW is observed. Given that the volume flow rate estimate is sensitive to the accepted value of cross-sectional area of the AW (see issue “a” above), the flow rate may be underestimated. One cannot also ignore the fact that horizontal density gradients of the geostrophic flow can be strengthened or weakened during the formation and passage of synoptic eddies, the influence of which on the average density field cannot be filtered out. According to (Perez-Hernandez et al., 2017) north of Svalbard (between 21 and 33°E) in September, 2013, a large difference was found in the estimates of geostrophic volume flow rate (from 0.53 Sv to 3.39 Sv) due to the passage of eddies and meandering of the flow. Våge et al. (2016) based upon geostophic velocities at two CTD sections across the boundary current near 30º E (September, 2012) evaluated a net AW volume flow rate of 1.6±0.3 Sv. Authors of this paper found evidence of a large eddy affecting the mean volume transport calculations.The barotropic velocity component, which is not taken into account in our estimates, can also affect the values of the volume flow rates. However, if the ice cover in the Eurasian Basin is high, the barotropic addition to the flow velocity cannot play a decisive role. In accordance to cruise reports, the NABOS CTD sections were characterized by the ice concentration of 50−100% (see https://uaf-iarc.org/nabos-cruises/). Exceptions occurred in the near-slope areas of the Laptev Sea, that is, in the sections along ~ 126ºE, where the ice concentration varied from 0 to 100%, having a maximum value in the northern part of the

sections. In such areas, the contribution of the barotropic component to the flow velocity can be very significant. For example, using long-term measurements (from 1995 to 1996) from a mooring in the near-slope area of the Laptev Sea, Woodgate et al. (2001) showed that the contribution of the barotropic component to the velocity of the Arctic Ocean Boundary Current (AOBC) was equal to the contribution of the first three baroclinic modes. To estimate the volume flow rate they assumed that the average velocity based on the measurements in the upper 1200 m layer was 4.5 cm/s and the horizontal extension of the flow was 50-84 km. At such values of the velocity and cross section of the flow the volume flow rate was estimated at 5 ± 1 Sv. This estimate differs from our average estimate of the AW volume flow rate along 126 ºE (0.39±0.22/±14, see Table 1) by an order of magnitude. Such a difference can be explained not only by the absence of a barotropic contribution in our case, but also by the fact that we took into account the average volume flow rate of the AW only (i.e. the cold, low-salinity surface layer was excluded) and considered certain season (August – September). Indeed, according to long-term measurements at 6 moorings on a section along 126 ºE, the AOBC volume flow rate varied from 0.3 Sv to 9 Sv (Pnyushkov et al., 2018 b). Such a wide range in volume flow rate estimates is probably due to a combined effect of seasonal variability and mesoscale eddies (Pnyushkov et al., 2018 a).

The fact that seasonal variations can in some cases significantly affect the AW volume flow rates (see also the discussion of different estimates of the AW volume flow rate in (Pnyushkov et al., 2018 b)) is confirmed by a number of observations (Schauer et al., 2002a; Beszczynska-Möller et al., 2012; Pnyushkov et al., 2018 b). For example, the volume flow rate of the AW in the northwestern part of the Barents Sea was 0.6 Sv according to velocity measurements in summer (Schauer et al., 2002a). This estimate agrees well with our estimate of the volume flow rate in the St. Anna Trough, 0.79 ± 0.22 Sv. However, the analysis of current velocity measurements in the winter season at the same section in the northwestern part of the Barents Sea gives a completely different estimate of ~ 2.6 Sv (Schauer et al., 2002a).

c) According to (Dmitrenko et al, 2009), the BSBW signal is satisfactorily identified at 142°E. However, a “pattern” in the θ-S diagram far from the place of the BSBW entry into the Eurasian Basin can be regarded as the BSBW signal, if it maintains the similarity with the “pattern” of the BSBW at the exit from the St. Anna Trough, that is, with the so-called “knee” (Dmitrenko et al., 2015). Our analysis showed that the “knee” is regularly observed at 103°E, while at 126°E it is either absent or weakens strongly and distorted. Apparently this is quite natural, since the flow velocity is small, and the BSBW covers a distance from 103°E to 126°E for 1−2 years. However, despite of such a long travel time, the other AW branch, the FSBW, is well identified not only at 126°E, but also further along the slope. It seems acceptable to

associate this situation with characteristic features of transformation and mixing of, primarily, the BSBW. The BSBW transformation can be due to various reasons, including mixing with the FSBW caused by thermohaline intrusive layering at absolutely stable stratification (Merryfield, 2002; Kuzmina et al., 2013; Kuzmina et al., 2014; Kuzmina, 2016, Zhurbas N., 2018; Kuzmina et al., 2018, 2019). Indeed, according to numerous studies, the intrusive layering in the ocean determines the processes of exchange and mixing of various water masses (see, e.g., Stern, 1967; Fedorov, 1976; Joyce, 1980; Zhurbas et al., 1993; Rudels et al., 1999; Kuzmina, 2000; Walsh and Carmack, 2003). Other reasons for the BSBW signal disappearance may be the following: the influence of the slope topography, the impact of local counterflows near the slope (see, for example, (Pnyushkov et al., 2015)), lateral convection (Ivanov and Shapiro, 2005; Ivanov and Golovin, 2007; Walsh et al., 2007), the impact of the Arctic Shelf Break Water (Aksenov et al., 2011; Ivanov and Aksenov, 2013) and mixing due to eddies (Schauer et al., 2002; Dmitrenko et al., 2008; Aagaard et al., 2012; Pnyushkov et al., 2018a). The understanding of the processes of transformation and mixing of the BSBW and FSBW is necessary to verify an important concept expressed in (Rudels, et al., 2015) that the BSBW supplies the major part of the AW to the Amundsen, Makarov and Canadian Basins, while the FSBW remains almost fully in the Nansen Basin.

5 Summary

The estimates of θ-S values and of the volume flow rate of the current carrying the AW in the Eurasian Basin were obtained based on the analysis of CTD data collected within the NABOS program in 2002–2015; additionally CTD transect PS-96 was considered. All estimates are given in tabular form.

It was found that the FSBW was satisfactorily identified at all transects, including the two transects in the Makarov Basin (159°E), while the cold waters at the transects along longitudes 126°E, 142°E and 159°E, which can be associated with the influence of the BSBW, were observed in the depth range below 800 m and had little effect on the spatial structure of isopycnic surfaces and horizontal gradient of density. It was shown using θ-S analysis that the BSBW signal, which is characterized by the knee-shape feature in coordinates θ, S and σ_Θ, S (see Fig.8), is either strongly weakened or not visible at the longitude 126°E (exluding the observations 2002 at 126 °E), while the FSBW signal is well identified at 126ºE and further along the slope of the Eurasian Basin. Based on the revealed features of the temperature, salinity and density fields, it is suggested that east of 126ºE the geostrophic volume flow rate of the AW is determined mainly by the FSBW.

A special attention was paid to the study of the variability of the geostrophic volume flow rate of the AW propagating along the continental slope of the Eurasian Basin and Makarov Basin. In order to assess spatial variability of the geostrophic volume flow rate, standard statistical analysis was used. It was shown with a 80% probability that the geostrophic volume flow rate increases from the region of 31ºE−92ºE (0.5 ± 0.14 Sv) to the region of 94ºE−107ºE (1.09 ± 0.38 Sv), then decreases to the region of 126ºE (0.39 ± 0.14 Sv) and becomes small (0.03 ± 0.1 Sv) in the Makarov Basin (159ºE).

A study of the temporal variability of hydrological parameters and of the volume flow rate is summarized as follows. The time series of θ_{max} had an absolute maximum in 2006–2008 that can be interpreted as a result of heat pulse in the early 2000s (Polyakov et al., 2011). In accordance with our analysis the time series of θ_{max} had a maximum in 2013 but only at the longitude 103°E (see also Table 1 and Fig.10). The time series of $S(\theta_{max})$ also display an increase of AW salinity in 2006–2008 and 2013, that can be referred to as a AW salinization in the early 2000s. Moreover the salinity increases almost monotonously in the period from 2003 to 2013 at 142ºE . It is important to underline also that the maxima of θ_{max} and $S(\theta_{max})$ in 2006 and 2013 (103°E) were accompanied by the volume flow rate highs. A significant increase in geostrophic volume flow rate identified in 2006 was shown to be caused by climate impact.

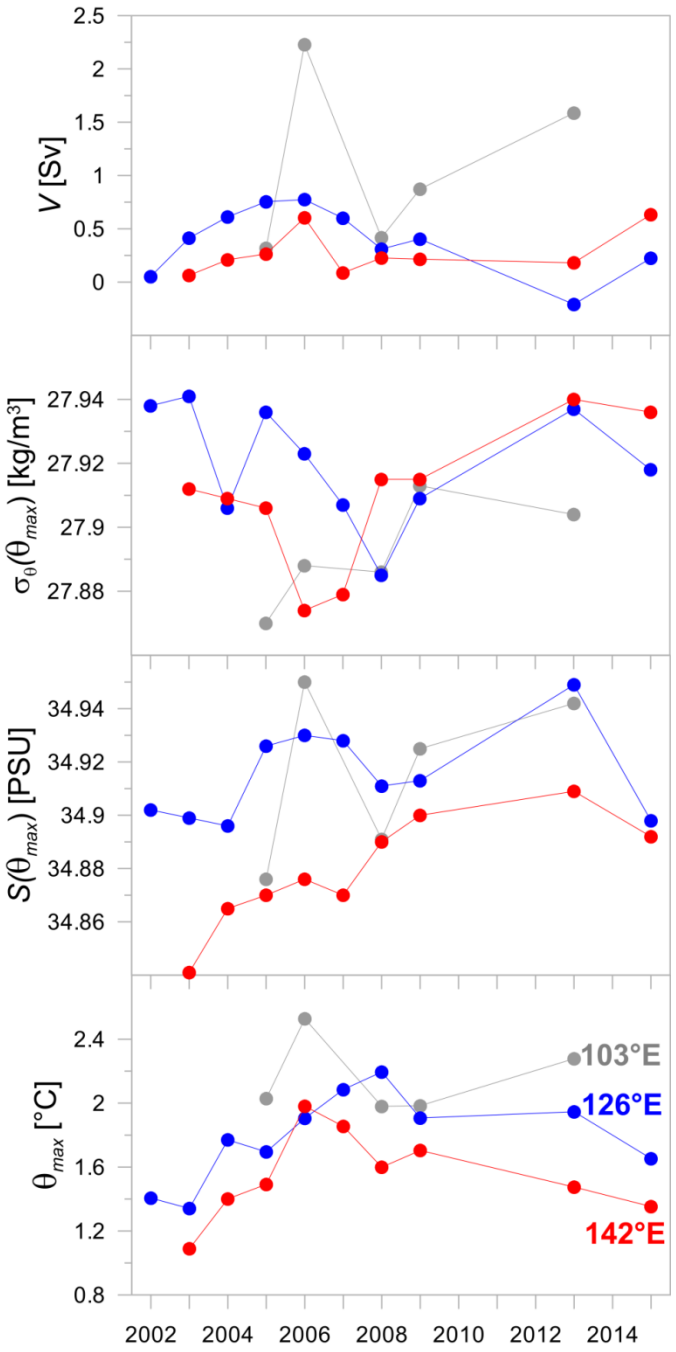

Fig. 10. Interannual variability of the maximum temperature θ_{max} and the related values of salinity $S(\theta_{max})$, potential density anomaly $\sigma_\theta(\theta_{max})$ and volume flow rate V on the cross-slope transects at 103°E, 126°E and 142°E.

Acknowledgments. This research, including the approach development, data processing and interpretation, performed by Nataliya Zhurbas, was funded by Russian Science Foundation, project no. 17-77-10080. Natalia Kuzmina (θ-S analysis, participation in discussion) was supported by the state assignment of the Shirshov Institute of Oceanology RAS (theme no. 0149-2019-0003). The authors are very grateful to the NABOS team for providing the opportunity to use the CTD-data.

References

Aagaard, K.: On the deep circulation of the Arctic Ocean, Deep-Sea Res., 28, 251–268, 1981.

Aagaard, K., and Carmack, E. C.: The role of sea ice and other fresh water in the Arctic circulation, J. Geophys. Res., 94(C10), 14485–14498, doi: 10.1029/JC094iC10p14485, 1989.

Aagaard, K., Andersen, R., Swift, J., and Johnson, J.: A large eddy in the central Arctic Ocean, Geophys. Res. Lett., 35, L09601, doi: 10.1029/2008GL033461, 2008.

Aksenov, Y., Ivanov, V. V., Nurser, A. J. G., Bacon, S., Polyakov, I. V., Coward, A. C., Naveira-Garabato, A. C., and Beszczynska-Moeller, A.: The Arctic Circumpolar Boundary Current, J. Geophys. Res., 116, C09017, 1–28, doi:10.1029/2010JC006637, 2011.

Arneborg, L., Fiekas, V., Umlauf, L., and Burchard, H.: Gravity current dynamics and entrainment – A process study based on observations in the Arkona Basin, J. Phys. Oceanogr., 37, 2094–2113, doi:10.1175/JPO3110.1, 2007.

Beszczynska-Möller, A., Fahrbach, E., Schauer, U., and Hansen, E.: Variability in Atlantic water temperature and transport at the entrance to the Arctic Ocean, 1997–2010, ICES Journal of Marine Science, 69(5), 852–863, doi: 10.1093/icesjms/fss056, 2012.

Dmitrenko, I. A., Kirillov, S. A., Ivanov, V. I., and Woodgate, R.: Mesoscale Atlantic water eddy off the Laptev Sea continental slope carries the signature of upstream interaction, J. Geophys. Res., 113, C07005, doi: 10.1029/2007JC004491, 2008.

Dmitrenko, I. A., Kirillov, S. A., Ivanov, V. V., Woodgate, R. A., Polyakov, I. V., Koldunov, N., Fortier, L., Lalande, C., Kaleschke, L., Bauch, D., Hölemann, J. A., and Timokhov, L. A.: Seasonal modification of the Arctic Ocean intermediate water layer off the eastern Laptev Sea continental shelf break, J. Geophys. Res.-Oceans, 114, C06010, https://doi.org/10.1029/2008JC005229, 2009.

Dmitrenko, I. A., Rudels, B., Kirillov, S. A., Aksenov, Y. O., Lien V. S., Ivanov, V. V., Schauer, U., Polyakov, I. V., Coward, A., and Barber, D. J.: Atlantic Water flow into the Arctic Ocean through the St. Anna Trough in the northern Kara Sea, J. Geophys. Res.: Oceans, 120(7), 5158–5178, doi: 10.1002/2015JC010804, 2015.

Fahrbach, E., Meincke, J., Osterhus, S., Rohardt, G., Schauer, U., Tverberg, V., and Verduin, J.: Direct measurements of volume transport through Fram Strait, Polar Res., 20(2), 217–224, doi: 10.1111/j.1751-8369.2001.tb00059.x, 2001.

Fedorov, K. N.: Physical Nature and Structure of Oceanic Fronts, Gidrometeoizdat, Leningrad, 296 pp., 1983 (in Russian).

Ivanov, V. V., and Shapiro, G. I.: Formation of dense water cascade in the marginal ice zone in the Barents Sea, Deep-Sea Res. Pt. I, 52, 1699–1717, doi: 10.1016/j.dsr.2005.04.004, 2005.

Ivanov, V., and Golovin, P.: Observations and modelling of dense water cascading from northwestern Laptev Sea shelf, J. Geophys. Res., 112, C09003, doi:10.1029/2006JC003882, 2007.

Ivanov, V. V., and Aksenov, E. O.: Atlantic Water transformation in the Eastern Nansen Basin: observations and modelling, Arctic and Antarctic Research, 1(95), 72–87, 2013 (in Russian).

Joyce, T. M.: A note on the lateral mixing of water masses, J. Phys. Oceanogr., 7(4), 626–629, 1980.

Kolås, E., and Fer, I.: Hydrography, transport and mixing of the West Spitsbergen Current: the Svalbard Branch in summer 2015, Ocean Sci., 14, 1603–1618, doi: 10.5194/os-14-1603-2018, 2018.

Kuzmina, N. P.: On the parameterization of interleaving and turbulent mixing using CTD data from the Azores Frontal Zone, J. Mar. Syst., 23(4), 285–302, 2000.

Kuzmina, N., Rudels, B., Zhurbas, V., and Stipa, T.: On the structure and dynamical features of intrusive layering in the Eurasian Basin in the Arctic Ocean, J. Geophys. Res., 116, C00D11, doi: 10.1029/2010JC006920, 2011.

Kuzmina, N. P., Zhurbas, N. V., and Rudels B.: Structure of intrusions and fronts in the deep layer of the Eurasian Basin and Makarov Basin (Arctic), Oceanology, 53(4), 410–421, doi: 10.1134/S0001437013040061, 2013.

Kuzmina, N. P., Zhurbas, N. V., Emelianov, M. V., and Pyzhevich, M. L.: Application of interleaving Models for the Description of intrusive Layering at the Fronts of Deep Polar Water in the Eurasian Basin (Arctic), Oceanology, 54(5), 557–566, doi: 10.1134/S0001437014050105, 2014.

Kuzmina, N. P.: Generation of large-scale intrusions at baroclinic fronts: an analytical consideration with a reference to the Arctic Ocean, Ocean Sci., 12, 1269–1277, doi: 10.5194/os-12-1269-2016, 2016.

Kuzmina, N. P., Skorokhodov, S. L., Zhurbas, N. V., and Lyzhkov, D. A.: On instability of geostrophic current with linear vertical shear at length scales of interleaving, Izv. Atmos. Ocean. Phys., 54(1), 47–55, doi: 10.1134/S0001433818010097, 2018.

Marnela, M., Rudels, B., Houssais, M.-N., Beszczynska-Mőller, A., and Eriksson, P. B.: Recirculation in the Fram Strait and transports of water in and north of the Fram Strait derived from CTD data, Ocean Sci., 9, 499–519, doi: 10.5194/os-9-499-2013, 2013.

Merryfield, W. J.: Intrusions in Double-Diffusively Stable Arctic Waters: Evidence for Differential mixing?, J. Phys. Oceanogr., 32, 1452–1459, 2002.

Pérez-Hernández, M. D., Pickart, R. S., Pavlov, V., Våge, K., Ingvaldsen, R., Sundfjord, A., Renner, A. H. H., Torres, D. J., and Erofeeva, S. Y.: The Atlantic Water boundary current

north of Svalbard in late summer, J. Geophys. Res.-Oceans, 122, 2269–2290, https://doi.org/10.1002/2016JC012486, 2017.

Pfirman, S. L., Bauch, D., and Gammelsrød, T.: The northern Barents Sea: water mass distribution and modification, in: The Polar Oceans and Their Role in Shaping the Global Environment, Geophysical Monograph 85, edited by: Johannessen, O. M., Muench, R. D., and Overland, J. E., American Geophysical Union, Hoboken, NJ, 77–94, 1994.

Pnyushkov, A. V., Polyakov, I. V., Ivanov, V. V., Aksenov, Ye, Coward, A. C., Janout, M., and Rabe, B.: Structure and variability of the boundary current in the Eurasian Basin of the Arctic Ocean, Deep-Sea Res. Pt. I, 101, 80–97, https://doi.org/10.1016/j.dsr.2015.03.001, 2015.

Pnyushkov, A. V., Polyakov, I. V., Padman, L., and Nguyen An T.: Structure and dynamics of mesoscale eddies over the Laptev Sea continental slope in the Arctic Ocean, Ocean Sci., 14, 1329–1347, https://doi.org/10.5194/os-14-1329-2018, 2018a.

Pnyushkov, A. V., Polyakov, I. V., Rember, R., Ivanov, V. V., Alkire, M. B., Ashik, I. M., Baumann, T. M., Alekseev, G. V., and Sundfjord, A.: Heat, salt, and volume transports in the eastern Eurasian Basin, Ocean Sci., 14, 1349–1371, https://doi.org/10.5194/os-14-1349-2018, 2018b.

Polyakov, I. V., Beszczynska, A., Carmack, E. C., Dmitrenko, I. A., Fahrbach, E., Frolov, I. E., Gerdes, R., Hansen, E., Holfort, J., Ivanov, V. V., Johnson, M. A., Karcher, M., Kauker, F., Morison, J., Orvik, K. A., Schauer, U., Simmons, H. L., Skagseth, Ø., Sokolov, V. T., Steele, M., Timokhov, L. A., Walsh, D., and Walsh, J. E.: One more step toward a warmer Arctic, Geophys. Res. Lett., 32, L17605, doi: 10.1029/2005GL023740, 2005.

Polyakov, I., Timokhov, L., Dmitrenko, I., Ivanov , V., Simmons , H., Beszczynska-Möller, A., Dickson, R., Fahrbach, E., Fortier, L., Gascard, J.-C., Hölemann, J., Holliday., N. P., Hansen, E., Mauritzen, C., Piechura, J., Pickart, R., Schauer, U., Walczowski, W, and Steele, M.: Observational program tracks Arctic Ocean transition to a warmer state, Eos Trans. AGU, 88(40), 398–399, https://doi.org/10.1029/2007EO400002, 2007.

Polyakov, I. V., Alexeev, V. A., Ashik, I. M., Bacon, S., Beszczynska-Möller, A., Carmack, E. C., Dmitrenko, I. A., Fortier, L., Gascard, J.-C., Hansen, E., Hölemann, J., Ivanov, V. V., Kikuchi, T., Kirillov, S., Lenn, Y.-D., McLaughlin, F. A., Piechura, J., Repina, I., Timokhov, L. A., Walczowski, W., and Woodgate, R.: Fate of Early 2000s Arctic Warm Water Pulse, Bulletin of the American Meteorological Society, 92(5), 561–566, doi: 10.1175/2010BAMS2921.1, 2011.

Polyakov, I. V., Pnyushkov, A., Rember, R., Ivanov, V., Lenn, Y-D., Padman, L., and Carmack, E. C.: Mooring-based observations of the double-diffusive staircases over the Laptev Sea, J. Phys. Oceanogr., 42, 95–109, doi: 10.1175/2011JPO4606.1, 2012.

Polyakov, I. V., Pnyushkov, A. V., Alkire, M. B., Ashik, I. M., Baumann, T. M., Carmack, E. C., Goszczko, I., Guthrie, J., Ivanov, V. V., Kanzow, T., Krishfield, R., Kwok, R., Sundfjord, A., Morison, J., Rember, R., and Yulin, A.: Greater role for Atlantic inflows on sea-ice loss in the Eurasian Basin of the Arctic Ocean, Science, 356, 285–291, https://doi.org/10.1126/science.aai8204, 2017.

Rudels, B.: On the mass balance of the polar ocean, with special emphasis on the Fram Strait, Skr. Nor. Polarinst., 188, 1–53, 1987.

Rudels, B., Jones, E. P., Anderson, L. G., and Kattner, G.: On the intermediate depth waters of the Arctic Ocean, in: The Role of the Polar Oceans in Shaping the Global Climate, edited by: Johannessen, O. M., Muench, R. D., and Overland, J. E., American Geophysical Union, Washington, DC, 33–46, 1994.

Rudels, B.: Aspects of Arctic oceanography, in Physics of ice-covered seas, vol. 2, edited by: Leppäranta, M., Univ. Press, Helsinki, 517–568, 1998.

Rudels, B., Björk, G., Muench, R. D, and Schauer, U.: Double-diffusive layering in the Eurasian Basin of the Arctic Ocean, J. Mar. Syst., 21(1–4), 3–27, doi: 10.1016/S0924-7963(99)00003-2, 1999.

Rudels, B., Jones, E. P., Schauer, U., and Eriksson, P.: Atlantic sources of the Arctic Ocean surface and halocline water, Polar research, 23(2), 181–208, doi: 10.1111/j.1751-8369.2004.tb00007.x, 2006.

Rudels, B., Kuzmina, N., Schauer, U., Stipa, T., and Zhurbas, V.: Double-diffusive convection and interleaving in the Arctic Ocean – Distribution and importance, Geophysica, 45(1–2), 199–213, 2009.

Rudels, B.: Arctic Ocean circulation, processes and water masses: A description of observations and ideas with focus on the period prior to the International Polar Year 2007–2009, Progress in Oceanography, 132, 22–67, doi: 10.1016/j.pocean.2013.11.006, 2015.

Rudels, B., Korhonen, M., Schauer, U., Pisarev, S., Rabe, B., and Wisotzki A.: Circulation and transformation of Atlantic water in the Eurasian Basin and the contribution of the Fram Strait inflow branch to the Arctic Ocean heat budget, Progress in Oceanography, 132, 128–152, doi: 10.1016/j.pocean.2014.04.003, 2015.

Schauer, U., Muench, R. D., Rudels, B., and Timokhov, L.: Impact of eastern Arctic shelf waters on the Nansen Basin intermediate layers, J.Geophysical Res., 102(C2), 3371–3382, 1997.

Schauer, U., Loeng, H., Rudels, B., Ozhigin, V. K., and Dieck, W.: Atlantic Water flow through the Barents and Kara Seas, Deep-Sea Res. Pt. I, 49(12), 2281–2298, https://doi.org/10.1016/S0967-0637(02)00125-5, 2002a.

Schauer, U., Rudels, B., Jones, E. P., Anderson, L. G., Muench, R. D., Björk, G., Swift, J. H., Ivanov, V., and Larsson, A.-M.: Confluence and redistribution of Atlantic water in the Nansen, Amundsen and Makarov basins, Ann. Geophys., 20, 257–273, doi: 10.5194/angeo-20-257-2002, 2002b.

Schauer, U., Fahrbach, E., Osterhus, S., and Rohardt, G.: Arctic warming through the Fram Strait: Oceanic heat transport from 3 years of measurements, J.Geophysical Res., 109(C06026), doi: 10.1029/2003JC001823, 2004.

Stern, M. E.: Lateral mixing of water masses, Deep-Sea Res., 14, 747–753, doi:10.1016/S0011-7471(67)80011-1, 1967.

Swift, J. H., Jones, E. P., Aagaard, K., Carmack, E. C., Hingston, M., MacDonald, R. W., McLaughlin, F. A., Perkin, R. G.: Waters of the Makarov and Canada basins, Deep-Sea Res. II, 44(8), 1503-1529, doi: 10.1016/S0967-0645(97)00055-6, 1997.

Våge, K., Pickart, R. S., Pavlov, V., Lin, P., Torres, D. J., Ingvaldsen, R., Sundfjord, A., and Proshutinsky, A.: The Atlantic Water boundary current in the Nansen Basin: Transport and mechanisms of lateral exchange, J. Geophys. Res., 121, 6946–6960, https://doi.org/10.1002/2016JC011715, 2016.

Walsh, D., and Carmack, E.: The nested structure of Arctic thermohaline intrusions, Ocean Model., 5, 267–289, doi: 10.1016/S1463-5003(02)00056-2, 2003.

Woodgate, R. A, Aagaard, K., Muench, R. D., Gunn, J., Bjork, G., B. Rudels, Roach, A. T., and Schauer, U.: The Arctic Ocean boundary current along the Eurasian slope and the adjacent Lomonosov Ridge: Water mass properties, transports and transformations from moored instruments, Deep-Sea Res. Pt. I, 48(8), 1757–1792, https://doi.org/10.1016/S0967-0637(00)00091-1, 2001.

Zhurbas, N. V.: On the eigenvalue spectra for a model problem describing formation of the large-scale intrusions in the Arctic Basin, Fundamentalnaya i Prikladnaya Gidrofizika, 11(1), 40–45, doi: 10.7868/S2073667318010045, 2018.

Zhurbas, N. V.: Estimates of transport and thermohaline characteristics of the Atlantic Water in the Eurasian Basin, Russian Meteorology and Hydrology, 2019 (Accepted).

Zhurbas, V. M., Kuzmina, N. P., Ozmidov, R. V., Golenko, N. N., and Paka, V. T.: Manifestation of subduction in thermohaline fields of vertical fine structure and horizontal mesostructure in frontal zone of Azores Current, Okeanologiya+, 33, 321–326, 1993.

Zhurbas, V., Elken, J., Paka, V., Piechura, J., Väli, G., Chubarenko, I., Golenko, N., and Shchuka, S.: Structure of unsteady overflow in the Słupsk Furrow of the Baltic Sea, J. Geophys. Res. – Oceans, 117, C04027, doi:10.1029/2011JC007284, 2012.